Title
Bioinspired structural color sensors based on responsive soft materials

Journal
Current Opinion in Solid State and Materials Science, 23(1)

ISSN
1359-0286

Authors
Qin, M
Sun, M
Hua, M
et al.

Publication Date
2019-02-01

DOI
10.1016/j.cossms.2018.10.001

Peer reviewed

Current Opinion in Solid State & Materials Science xxx (xxxx) xxx–xxx

Contents lists available at ScienceDirect

Current Opinion in Solid State & Materials Science

journal homepage: www.elsevier.com/locate/cossms

Bioinspired structural color sensors based on responsive soft materials

Meng Qin, Mo Sun, Mutian Hua, Ximin He*

Department of Materials Science and Engineering, University of California, Los Angeles, CA 90095, USA

ARTICLE INFO

Keywords:
Bioinspired
Structural color
Synthetic polymer
Natural material
Chemical sensing
Biosensing
Multi-analyte discrimination

ABSTRACT

Structural colors in nature have inspired the design of diverse photonic structures, which can interact with light via interference, diffraction or scattering. Among them, responsive soft material-involved photonic structures uniquely feature large volumetric changes upon external stimuli. The volumetric changes result in peak/valley shift of reflection spectra and perceptible color changes, providing responsive soft material-based structural color systems capability of serving as sensors for detecting chemical and biological analytes. Synthetic polymers and some natural materials are the most studied and utilized responsive soft materials for constructing structural color sensors, by tuning the thickness and morphology of formed films, or incorporating them into template structures, or their self-assembling. In this review article, structural colors in nature are firstly introduced, followed by discussing recent developments of promising responsive soft material-based structural color sensors, including the design of structural color sensors based on synthetic polymers and natural materials, as well as their applications for chemical sensing, biosensing, and multi-analyte sensing with sensor arrays. For specific sensing of chemicals and biomolecules, the sensing performance is evaluated in terms of detection range, sensitivity, response time, and selectivity. For multi-analyte sensing, cross-reactive structural sensor arrays based on simply a single soft material will be shown capable of discriminating various series of similar compounds. The future development of structural color sensors is also proposed and discussed.

1. Introduction

The prevalence of smart technologies nowadays has boosted the emergence of point-of-care and personalized healthcare products, including wearable devices (*e.g.*, head/wrist bands, patches, and contact lens) for monitoring metabolism or other health conditions of general public, athletes, or patients [1,2]. Real-time monitoring of the air quality and natural or waste water without the requirement of the access to analytical laboratory or large-scale instrument is desirable for broad environment safety and protection [3]. To meet these increasing demands from health and environmental fields, tremendous research efforts have been taken on the innovation of low-cost, high-performance and easy-to-use detections of chemical and biological molecules in gaseous and liquidus phases [4,5]. As one of the most promising methods, colorimetric sensors provide visual or optically detectable readout signals, arising from the distinct color changes of the stimuli-responsive materials which serve as the key active element of the sensors in presence of different analytes [6]. The optical readout can be easily read by imager and even naked eyes and further analyzed by mobile devices quantitatively, which facilitates user-friendly monitoring of health and environment [7–9]. With these advantages, optical chemical/biological sensors have been playing an important role in transforming biomedical, environmental and security fields, as emerging technologies for rapid diagnostics, cost-efficient disease and drug prescreening, as well as real-time environment monitoring [10,11]. For example, an ultrasensitive and selective optical sensor has been used for the detection of copper ions, which is of importance for the monitoring of seawater quality, since free copper ions in ocean should be critically maintained between picoM ~ femtoM (10^{-12}–10^{-15} M) to be micronutrients for organisms [12].

Based on the sensing materials and mechanisms of color generation, colorimetric sensors can be generally classified into chromophore- and dye-based, plasmonic nanoparticle-based, and structural color-based sensors [13–15]. Among these types, structural color sensors exhibit colors that arise from interaction of incident light and the micro/nanostructures via interference, diffraction or scattering of the light beams. Most of the micro/nano-structures are the interior structures, while microstructure changes on the surface of the materials have been shown effective in producing optical readout sensors as well [16]. Sensing signals which come from optical spectrometry (*e.g.* reflection peak/valley in the wavelength range of 400–800 nm) and/or color model analysis (*e.g.* RGB color analysis) are used for qualitative and

* Corresponding author.
E-mail address: ximinhe@ucla.edu (X. He).

https://doi.org/10.1016/j.cossms.2018.10.001
Received 28 July 2018; Received in revised form 1 October 2018; Accepted 4 October 2018

quantitative detection. Compared with chromophore- and dye-based sensors, structural color sensors possess the advantage of non-faded and dynamic colors, while they are cost-effective compared with plasmonic nanoparticle-based sensors. Basically, the design strategy of structural color sensors combines the construction of photonic structures and the employment of responsive materials. To achieve stimuli-responsive color alterations for high-performance detection, it requires responsive materials capable of changing their photonic structures significantly upon exposure to analytes. Responsive soft materials can volumetrically expand or contract significantly in response to external stimuli, providing great potential to serve as responsive materials to vary photonic structures and produce color changes. Synthetic polymers are the typical and most studied soft materials utilized in structural color systems, by functionalizing their polymeric network to respond to numerous stimuli, such as light, temperature, mechanical stress and chemicals. In addition to synthetic polymers, natural materials have been recently introduced to construct responsive structural color systems due to their advantages of biocompatibility and biodegradability.

In this review article, we firstly introduced the structural colors in nature to reveal the optical structures that inspire the design of structural color sensors. Then we summarized recent progress on structural color sensors by using synthetic polymers (including hydrogels, liquid crystal polymers, and block copolymers) and some natural materials. The properties of the materials and corresponding strategies (focused on “bottom-up” methods) to design structural color sensors are discussed. Based on these sensors, achievements since 2014 on chemical sensing and biosensing, specifically their analyte types, detection range, sensitivity, response time, and selectivity, are summarized, followed by a highlight of development of structural color sensor arrays for multi-analyte discrimination, which has attracted much attention in recent years. Lastly, the outlook of the future directions of structural color sensors is described.

2. Structural colors in nature

The design of photonic structures can be learnt from many living organisms in nature, which display vivid structural colors through interference, diffraction, and scattering. These three types of structural colors in nature and their corresponding nature-inspired colorimetric sensors are respectively described as follows. The simplest case is thin-film interference-based color, which originates from the interaction of optical waves reflected by the upper and lower interfaces of a thin layer with thickness comparable to visible light wavelength. For example, the transparent wings of numerous insets are composed of two layers of chitin, on which light is reflected by the upper and lower surfaces, generating interference colors (Fig. 1a) [17]. For the thin-film interference, the color is determined by constructive interference, which obeys

$$2n_2 d\cos\theta = (m-0.5)\lambda \quad (1)$$

where n_2 is the refractive index and d is the thickness of the thin film, θ is the angle of incident wave, λ is the wavelength of interference light, and m is an integer (Fig. 1b) [18]. When the film is attached to a layer with a higher refractive index, the constructive interference is governed by

$$2n_2 d\cos\theta = m\lambda \quad (2)$$

In the reflection spectral wavelength range of 400–800 nm, there may be multiple constructive interference locations, due to multi-order diffraction. Thus, the interference color is a combination of multiple reflection peaks/valleys in the reflection spectrum.

In addition to this thin-film interference color, living organisms show diffraction-induced color through the interaction of light and periodic structures, named photonic crystals (PCs). PCs, ranging from one dimensional (1D), two dimensional (2D), to three dimensional (3D) structures, can control the propagation of incident light through the alternatively arranged materials with different refractive indices and lattice spacing comparable to visible light wavelength. The perceptible color is determined by a single peak (photonic band gap) in the reflection spectrum. Fig. 1c–f show 1D biological PC structures, of which Fig. 1c and d demonstrate multilayer interference induced green color of the elytron of longhorn beetle *Tmesisternus isabellae* [19], and Fig. 1e and f exhibit the color of flower *Hibiscus trionum* with the corresponding 1D diffraction gratings [20]. 2D PC structures are ordered lattices that materials are periodically arranged in a 2D space and can be found on many marine creatures. The comb-jellyfish *Beroë cucumis* is a transparent marine animal, but it can be recognized by the iridescence of comb rows, which originate from regular packing of the cilia to an orthorhombic lattice (Fig. 1g and h) [21]. Some species show colors from 3D PC structures, in which the periodicity remains in all three directions. The most commonly studied 3D PC is opal structure, which can also be found on the weevil *Pachyrhynchus argus* (Fig. 1i and j). The yellow-green color of the patches on its body comes from the hexagonal close-packing array of transparent spheres [22]. Besides these PCs, some animals even possess more complicated PC structures, such as the diamond structures on some beetle cuticles [23] and the gyroid structures on some butterfly wings (Fig. 1k and l) [24]. These structures are composed of non-self-intersecting networks of periodically arranged bicontinuous phases, with the crystallographic space group symmetry [25]. Similar to the physics of thin-film interference color, all PC-based structural colors are determined by the refractive indices of constructive materials and the lattice spacing, when the viewing angle is fixed.

As discussed above, structural color changes can be induced by the variations of refractive indices and the volume or sizes of the constructive materials when the viewing angle remains unchanged. Many creatures have demonstrated these structural-color-changing mechanisms. The elytron of the beetle *Dynastes hercules* changes from khaki-green to black when humidity increases, due to water infiltration into

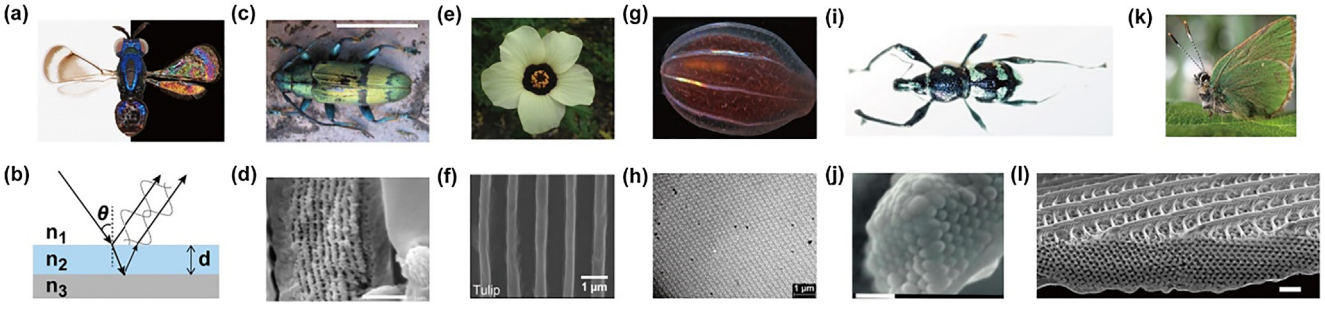

Fig. 1. Structural colors in nature. (a and b) Thin-film interference colors of inset wings [17] and the schematic illustration of light propagation. (c and d) Multilayer interference color of the elytron of longhorn beetle *Tmesisternus isabellae* [19]. (e and f) 1D diffraction gratings on flower *Hibiscus trionum* [20]. (g and h) 2D PC structure of the comb rows of comb-jellyfish *Beroë cucumis* [21]. (i and j) 3D PC structure of the patches on weevil *Pachyrhynchus argus* [22]. (k and l) Gyroid structure of the wings of butterfly *Callophrys rubi* [24].

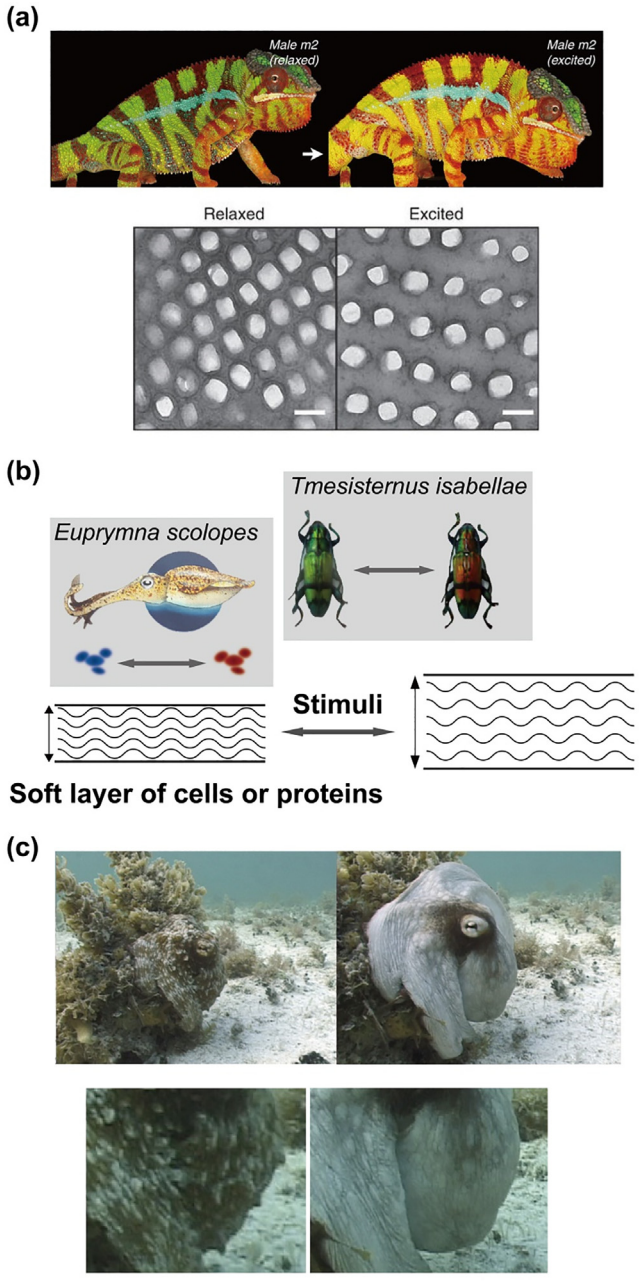

Fig. 2. Volume-change-induced structural color alteration in nature. (a) Chameleon *Furcifer pardalis* changes its skin color by tuning the lattice spacing of guanine nanocrystals in S-iridophores under the epidermis [27]. (b) The thickness change of the soft cell or protein layer causes color change of squid *Euprymna scolopes* and longhorn beetle *Tmesisternus isabellae* [9]. (c) Octopus changes skin texture for camouflage, by changing papillae on the skin surface [30].

the porous multilayer under its cuticle which consequently alters the refractive index of the multilayer structure [26]. Different from the refractive-index-induced color changes, the chameleon *Furcifer pardalis* changes its skin color from green to yellow/orange when it is exited, by tuning the lattice spacing of guanine nanocrystals in S-iridophores under the epidermis (Fig. 2a) [27]. This color change relies on the change in the soft layer of cells or proteins, which is also seen in many other animals. For example, as shown in Fig. 2b, the squid *Euprymna scolopes* can tune its skin color through thickness change of the reflectin platelet stacks in iridophores [16,28], while the melanoprotein layer in the elytron of longhorn beetle *Tmesisternus isabellae* can absorb water and swell [29]. Compared with refractive index altering induced color shift, the volume variation of the soft layer can result in more remarkable and sensitive color change (hue).

Beyond the internal microstructural changes, it has been found that the surface microstructure formation or changes on the soft tissues (*e.g.* wrinkle and/or creases) induced by volume changes can cause scattering and brightness variation, which may serve as a non-conventional optical readout to reflect the internal microenvironment change. For example, octopuses are able to change their skin texture in three dimensions for camouflage, which benefits from skin papillae change and resulting in variations of skin brightness and appearance (Fig. 2c) [30]. This mechanism has inspired the design of reflected-light-intensity-based structural color sensors.

3. Responsive soft materials for the design of structural color sensors

3.1. Synthetic polymers

3D synthetic polymeric networks can undergo volume change through solvent uptake and/or molecular reconfiguration, making them ideal materials to incorporate in designing structural color sensors. By controlling the composition of polymer chains, synthesis and fabrication methods, additives, etc., polymers can be assembled into the photonic structures discussed above. On the other hand, as-prepared photonic structures, such as colloidal crystal arrays, can serve as templates for embedding polymers, resulting in dynamic structural color systems [31]. The most popular and promising synthetic polymer materials used for structural color sensors are hydrogels, liquid crystal polymers, and block copolymers, which are also the focus of this section. Through functionalization of the networks, synthetic polymers can be controlled to respond to various chemical and biological stimuli.

3.1.1. Hydrogels

Hydrogels are cross-linked hydrophilic polymeric networks which can absorb water or various molecules and swell. The molecule diffusion in and out of the gel network leads to reversible and large degrees of volume phase transition. Different molecules can induce distinct volume change, which are inherently determined by the affinity/interaction between the molecules and hydrogel polymer chains [32]. The equilibrium state of swelling of hydrogels is the result of the balance between the Donnan osmatic pressure within hydrogel networks and elastic retractive forces of the polymer chains [33]. When water diffuses into the networks, the polymer chains would be hydrated and relaxed, leading to the expansion of the entire network; meanwhile, the stretching of polymer chains increases elastic retractive forces against the expansion. The swelling would reach equilibrium when these forces are balanced. If the hydrogel networks are functionalized with binding units, such as ionic groups and enzymes, corresponding analytes can interact with the polymer chains, causing changes in polymer composition or crosslinking density. As a result, the balance is disrupted, accompanied by the change of equilibrium volume. This molecular interaction is reflected in the macroscopic volume change of hydrogels, making them sensitive to a small alteration of environmental cues.

Different strategies have been developed to incorporate hydrogels in structural color systems. He et al. reported a simple and universal hydrogel thin-film interferometer as an adaptive color platform [9,12]. Through spin-coating and in-situ polymerization of hydrogel precursor solution, the fabrication of hydrogel interferometer can be completed within minutes. As shown in Fig. 3a, the hydrogel interferometer is composed of a single hydrogel layer covalently bonded to a reflective substrate. Based on thin-film interference theory, the color of the hydrogel interferometer is generated by the interference of two reflected optical waves from the air-hydrogel and hydrogel-substrate interfaces. With well-controlled hydrogel thickness at hundred-nanometer scale, the hydrogel interferometer can display a wide range of vibrant colors

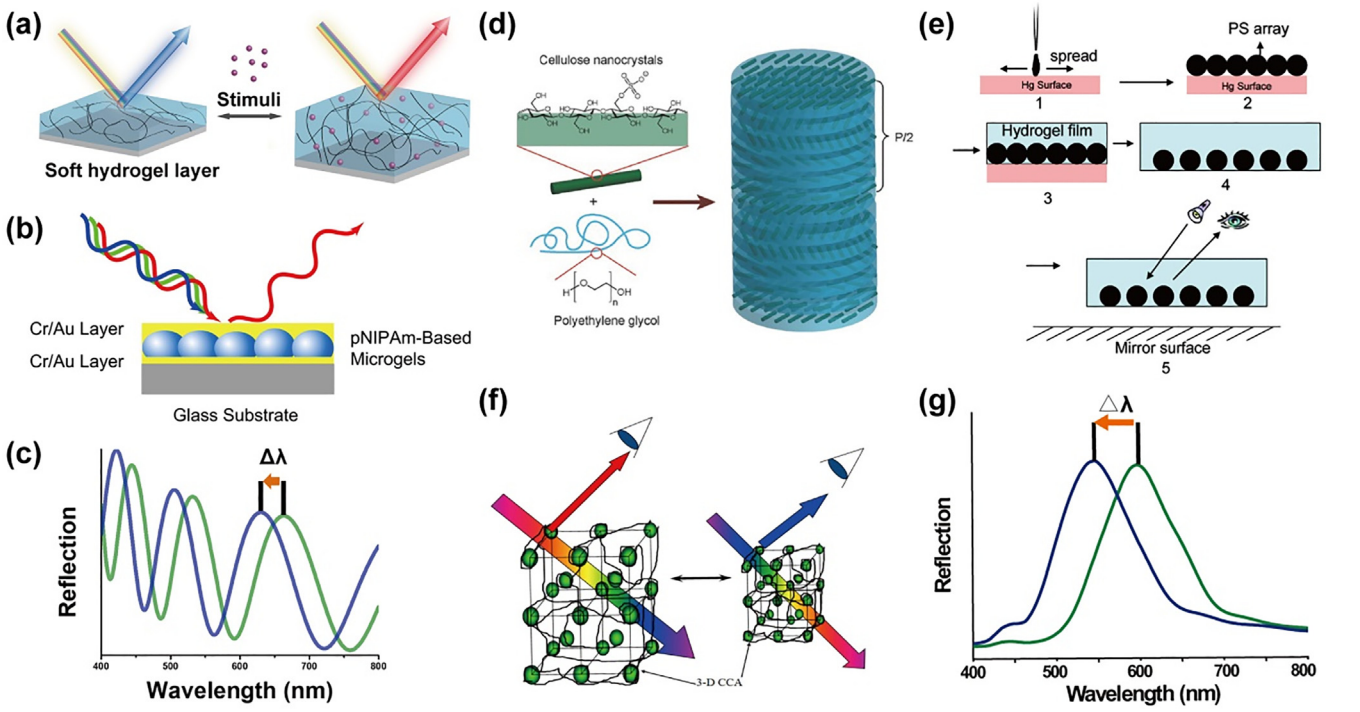

Fig. 3. Strategies to design hydrogels based structural color sensors. (a) Hydrogel interferometer based on a single hydrogel layer covalently bonded to a reflective substrate [9]. (b) Microgel etalon by sandwiching a microgel layer between two reflective surfaces [35]. (c) Typical reflection spectrum of (a) and (b). △λ is the shift of the location of constructive interference upon external stimuli. (d) 1D PC hydrogel based on CNCs template [38]. (e) 2D PC hydrogel based on monolayer of self-assembled PS particles [40]. (f) 3D PC hydrogel based on opal structure template [44]. (g) Typical reflection spectrum of (d)–(f). △λ is the shift of the location of photonic band gap upon external stimuli.

continuously. Upon external stimuli, the hydrogel layer instantly swells, leading to a color change and reflection shift (Fig. 3c) that can reveal rich environmental metrics, both quantitatively and qualitatively. The submicron-scale thickness of the hydrogel layer enables ultrashort diffusion length and fast diffusion of analytes to achieve equilibrium of swelling. As a result, the hydrogel interferometer shows response and recovery time at sub-second scale. By altering the hydrogel components, various analytes can be detected by the hydrogel interferometer. This simple and inexpensive fabrication method provides an effective way to construct colorimetric sensors.

In addition to the hydrogel thin-film, hydrogels can be shaped into micro/nano gels (*i.e.* gel particles) as the building blocks of forming the responsive layers, which show faster response compared with bulk hydrogels due to the reduced gel size. These hydrogel particles can self-assemble into a thin layer, which can be utilized to design dynamic color systems. Serpe et al. reported microgel etalons by sandwiching a microgel layer between two reflective surfaces (deposited Cr-Au layer) [34,35]. As shown in Fig. 3b, the incident light enters the dielectric cavity and resonate between the two reflective surfaces, thus, the microgel etalon generates color also according to the thin-film interference physics. When the microgel responds to analytes and swells, the color of the etalon alters with reflection shift (Fig. 3c).

A typical strategy of introducing hydrogels into structural color systems is the template-assisted method, usually with template of PC assembly. For “bottom-up” fabrication, two methods can be adopted to achieve structural coloration, the simplest of which is the co-assembly of polymer matrix and colloidal crystals. The alternative approach is to construct 1D, 2D, or 3D PC structure firstly through colloidal crystal assembly, followed by infiltration of hydrogel precursor solution into the voids and subsequent polymerization. With either of these two methods, the PC structure is fixed in the hydrogel matrix. The PC template can be retained in the hydrogel structural color system to form colloidal particle-hydrogel composite or removed through solvent etching to leave periodically arranged pores in the hydrogel matrix. The resulting structure shows a single reflection peak, which is the location of photonic band gap (Fig. 3g). A variety of materials have been reported to serve as colloidal templates of structural color systems, for example, superparamagnetic nanocrystal clusters [36]. Recently, cellulose nanocrystals (CNCs) are emerging as a promising 1D material for structural color templates. Extracted from natural cellulose fibrils by acid (*e.g.* sulfuric acid) hydrolysis, CNCs are nanorods capable of self-assembling to achieve structural colors. During slow drying of colloidal CNC suspensions, the randomly orientated nanorods tend to align in a cholesteric phase, possessing helical structure and reflecting left-handed polarized light [37]. Via stabilization of the cholesteric phase in hydrogel matrix, the iridescent CNCs/hydrogel nanocomposites are formed (Fig. 3d) [38]. The reflected light wavelength λ depends on

$$\lambda = nP\cos\theta \tag{3}$$

where n is the average refractive index of the nanocomposite, P is the helical pitch (*i.e.* distance for a full 360° turn of the nanorods), and θ is the incident angle of light [39]. When responding to stimuli, the swelling of embedded hydrogel causes the increase of the helical pitch, inducing a red-shift of the reflective wavelength, while the shrinkage of the hydrogel matrix leads to a blue-shift of the reflective wavelength.

In addition to 1D PC structure template, 2D and 3D colloidal crystal arrays have also been widely applied in templated structural color systems. Asher et al. have demonstrated a series of 2D and 3D PC hydrogel films. As shown in Fig. 3e, to fabricate 2D PC hydrogels, polystyrene (PS) particles with diameter of several hundred nanometers are firstly deposited onto Hg or water surface [40]. The PS particles would self-assemble into ordered 2D monolayer during the evaporation of solvent. Then the 2D PS array is transferred onto a substrate by either draining the water or by lifting a substrate from the liquid-air interface, and subsequent depositing the 2D array on the substrate. Consequently, the 2D PC template is formed. By infiltration of hydrogel precursor solution into the template followed by polymerization, the 2D PC hydrogel film is achieved. Due to the light diffraction within the 2D PC

structure, bright colors can be observed. The diffracted wavelength is proportional to the spacing between particles when the incident angle is defined. Swelling or shrinking of hydrogel matrix can cause particle spacing variation and produce colorimetric sensing signals. Compared with 2D PC hydrogels, 3D PC hydrogel films are more widely developed. Typically, 3D PC templates are also fabricated using PS or SiO_2 particle self-assembly. The particles self-organize to 3D opal structure by various methods, such as dip-coating [41], spin-coating [29], microfluidics [42] and inkjet printing [43]. After the evaporation of the suspension solvent and the infiltration of hydrogel, 3D PC hydrogel films or beads are formed. In response to external stimuli, the hydrogel matrix changes its volume, leading to alteration of the lattice spacing and the structural color (Fig. 3f) [44].

3.1.2. Liquid crystal polymers

Liquid crystal polymers are polymeric networks containing liquid crystalline molecules (*i.e.* mesogens) that form a mesophase between isotropic liquid state and crystalline solid state. Due to the self-assembly of liquid crystalline molecules, ordered structure can be achieved and frozen in the polymeric networks, providing structural colors. Among the different types of liquid crystalline phases (*i.e.* nematic, smectic, and cholesteric phases), thermotropic cholesteric liquid crystals (CLCs), which are also referred to chiral nematic liquid crystals (Fig. 4a), are most commonly employed into polymeric networks to serve as structural color sensors. Same as described for CNCs, the CLCs possess helical structure and selectively reflect incident light governed by Eq. (3), in which the average refractive index is

$$n = \frac{n_o + n_e}{2} \tag{4}$$

where n_o and n_e are the ordinary and the extraordinary refractive indices, respectively. The cholesteric phase can be formed from nematic alignment of rod-like molecules, by addition of a small amount of chiral dopant, whose ability to induce twisting is considered as helical twisting power (HTP) [45]. Chiral dopant molecules with more asymmetric chiral fragments are characterized by higher HTP. The relationship between HTP and helical pitch P is governed by

$$P = \frac{1}{\beta \times ee \times c} \tag{5}$$

where β is HTP, ee is enantiomeric excess, and c is the concentration of chiral dopant. To achieve visible structural color of CLCs, it is necessary to control the concentration of chiral dopant, ensuring the pitch length is comparable to visible light wavelength. The helical pitch of CLCs is sensitive to external stimuli; increase of the helical pitch induces red-shift of reflection peak (corresponding to the transmission peak in Fig. 4b), while decrease of the helical pitch results in blue-shift of reflection peak.

By crosslinking reactive CLCs mesogens with acrylate groups to 3D networks, CLC polymer is achieved. A widely used strategy to design CLC polymer-based structural color sensors is to introduce hydrogen bonds into the polymeric networks. An example of hydrogen-bonded CLC polymer is shown in Fig. 4c and d, which is demonstrated by Shibaev et al. [46]. 1,4-di(4-(6-acryloyloxyhexyloxy)benzoyloxy)benzene (DIAB) (2 in Fig. 4d), (6-hexaneoxy-4-benzoic acid) acrylate (HBA) (1a), methyladipic acid (MAA) (3), and 4-methoxyphenyl-4-(6-acryloyloxyhexyloxy)benzoate (HA1) (1) are nematic cross-linker, hydrogen donor/acceptor moiety, chiral dopant, and nematic monomer, respectively. The monomer mixtures show cholesteric state at temperature of *ca.* 70–90 °C. When the weight concentration of MAA exceeds 12–14%, visible structural color can be obtained. By photo-induced polymerization, the cholesteric mixtures form CLC polymer matrix with hydrogen bonds between MAA and HBA. External stimuli, *e.g.* pH change [47] or alcohols [48], would influence the strength of the hydrogen bonds, leading to the change of helical pitch length and thus a color shift of the polymer. Compared with hydrogels which are easily functionalized to diverse analytes, the stimuli capable of inducing response of CLC polymers are limited. Hence, interpenetrating CLC-

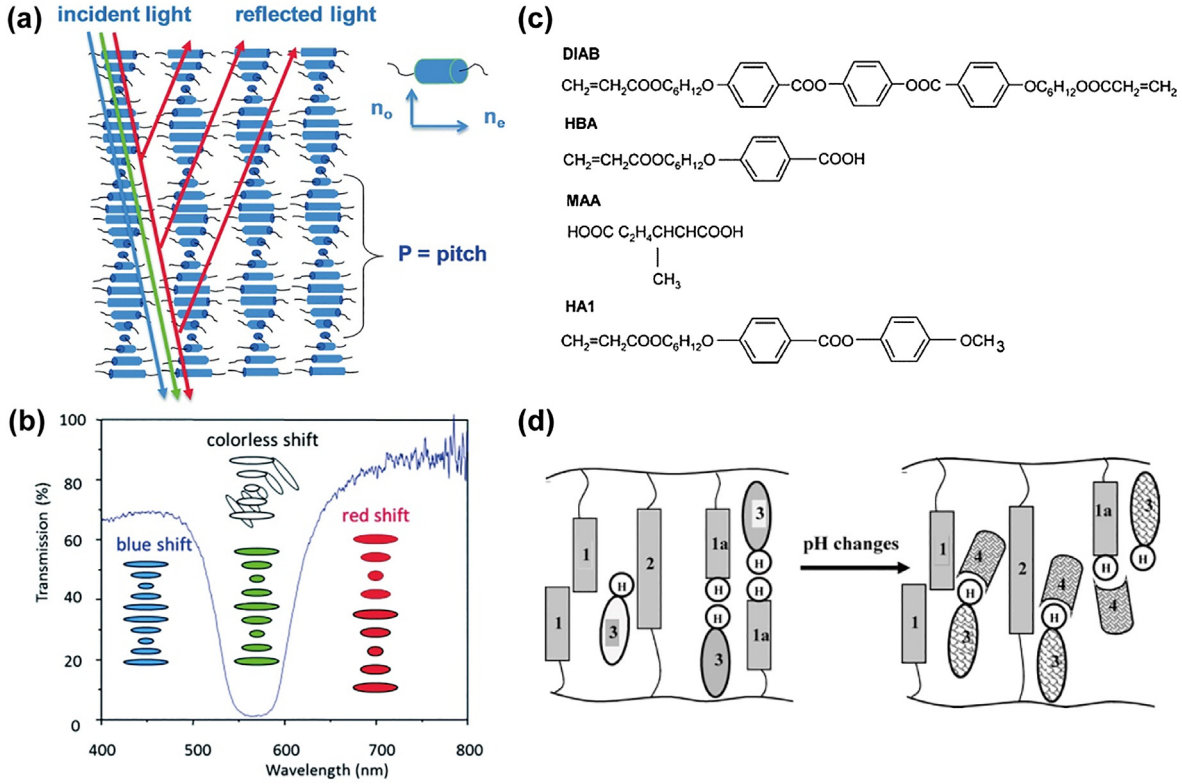

Fig. 4. (a) Light reflection and (b) transmission spectrum of CLCs. Increase of the helical pitch induces red-shift of the transmission peak, while decrease of the helical pitch results in blue-shift of the transmission peak [45]. (c) Monomer mixtures and (d) stimuli response of hydrogen-bonded CLC polymer [46].

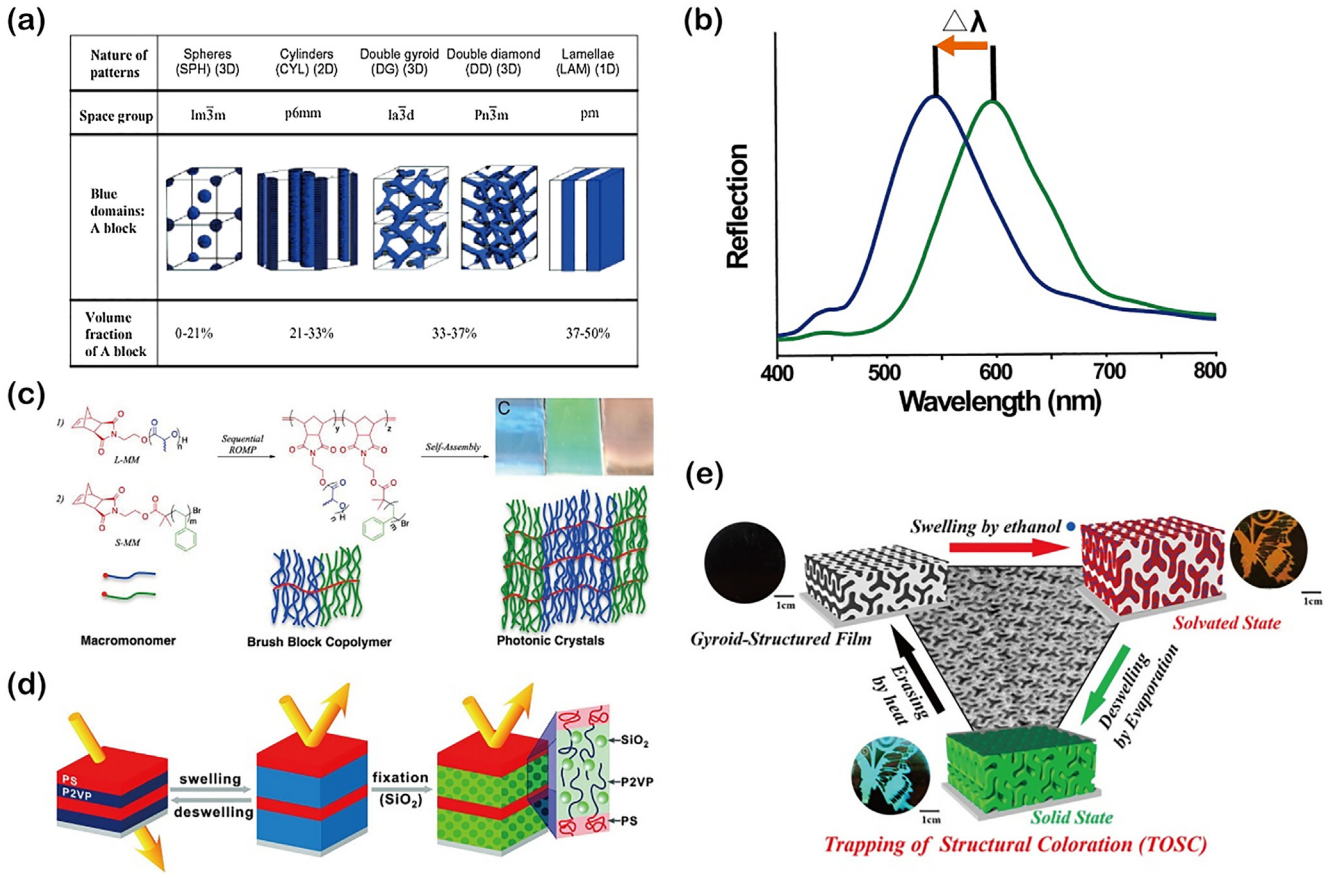

Fig. 5. (a) Microdomain geometries of AB diblock copolymer depending on the volume fraction of the two blocks [51]. (b) Typical reflection spectrum of BCP self-assemblies based structural color sensors. △λ is the shift of the location of photonic band gap upon external stimuli. (c) Lamellar PC films achieved from self-assembly of brush BCP [53]. (d) Lamellar PS-*b*-P2VP film reflected visible light by freezing the swollen film with SiO_2 gel networks [55]. (e) Trapping coloration of a gyroid-structured PS-*b*-P2VP film by ethanol [56].

hydrogel polymer networks have been designed to achieve wider response [49].

3.1.3. Block copolymers

Block copolymers (BCPs), which contains two or more homopolymer subunits linked by covalent bonds, are another type of synthetic polymers widely used in constructing structural color systems. Due to the chemical incompatibilities between different blocks, the positive free energy of mixing drives the segregation of respective blocks; on the other hand, restricted by the connectivity between the blocks, the BCP micro-phases separate into alternatively arranged microdomains, spontaneously forming PC structure at nanoscopic length scale [50]. The simplest BCP architecture is linear-AB-type diblock copolymer, which is composed of covalently bonded type A monomer sequence and type B monomer sequence. Microphase separation of the AB diblock copolymer can result in different geometries of microdomains, depending on the volume fractions of the two blocks [51]. As shown in Fig. 5a, with the increased volume fraction of A block in the range of 0–33%, the microdomain structure of AB diblock copolymer changes from spheres to cylinders. Within 33–37% volume fraction of A block, a bicontinuous phase, *i.e.* double gyroid or double diamond structure, occurs for the AB diblock copolymer. Increasing the volume fraction of A block to 50% would induce its transition into lamellae structure.

The major problem of using BCPs as colorimetric sensors is that the small refractive index contrast between the blocks and domain sizes are insufficient to achieve visible structural colors, which is corresponding to the reflection peak in Fig. 5b. To address this issue, increasing the sizes of the microdomains is usually employed. It has been reported that ultrahigh molecular weight (MW) linear BCPs (MW ≈ 10^6 g/mol) with a narrow molecular weight distribution can form large domains and exhibit visible structural colors [52]. However, the chain entanglement induces a large kinetic barrier in the self-assembly process, requiring a solvent with matching solubility and a considerably slow evaporation rate to drive the formation of ordered structures. Brush BCPs are alternatives to reduce the chain entanglement. Grubbs et al. synthesized high-MW brush BCP by ruthenium (Ru) mediated ring-opening metathesis polymerization (ROMP) to achieve lamellar PC films [53,54]. As shown in Fig. 5c, the polymer side-chains align parallelly with the lamellae and induce steric congestion to the backbone, giving rise to large equilibrium scaling and fast equilibration rates for the self-assembled structures. The reduced chain entanglement lowers the requirement of solvents to realize ordered structure; dichloromethane and tetrahydrofuran can both drive the self-assembly to form lamellar structure and visible coloration.

Instead of using high-MW BCPs for structural color sensors, BCPs with moderate-MW can achieve enlarged domain sizes and visible colors via swelling of polymer chains in selective solvents. With the large domain sizes frozen within the structures, solid-state BCP films with visible structural colors can be realized. Kang et al. froze the domain size by doping the microstructure with inorganic component [55]. As shown in Fig. 5d, lamellar structure is formed by spin-casting and solvent annealing of moderate-MW polystyrene-*block*-poly(2-vinyl pyridine) (PS-*b*-P2VP) BCP. After immersing the film in P2VP-selective methanol solvent, the P2VP domains swell by 5.5 times, resulting in visible blue color of the film. Then tetraethoxysilane is added in the methanol bath and infiltrate into P2VP domains, followed by hydrolyzation to form SiO_2 colloidal particles, which finally aggregate into a

continuous SiO_2 gel network. After drying, the swollen state is frozen in the BCP film. Recently, Chiang et al. reported coloration of a gyroid structure PS-*b*-P2VP BCP film by adding ethanol to the film, which can swell P2VP domains (Fig. 5e) [56]. During evaporation of ethanol, the P2VP chains reach the glass transition temperature (T_g), forming a glassy layer on the surface of the film. The stretched P2VP chains are maintained in the film after completely drying, leading to a visible structural color of the solid-state BCP film. When heated at temperature of 110 °C, the color disappears due to the reversion of the gyroid lattice size.

3.2. Natural materials

In recent years, natural materials, *e.g.* proteins and phages, have attracted much attention in fabrication of structural color sensors, attributed to their biocompatibility, biodegradability, and stimuli-responsiveness. Through template-assisted methods or self-assembly of these natural materials, photonic structures with vivid colors can be realized. Similar to synthetic polymers, these natural materials can change their volumes, leading to color alteration. Here we introduce three types of promising natural materials in fabrication of structural color sensors, *i.e.* reflectin, silk fibroin, and phage.

Reflectins are the proteins that give the iridescent color of cephalopods (*e.g. Euprymna scolopes*) through their self-assembly into platelet structure. After expressing, purifying, and diluting recombinant reflectins, it was found that the proteins tended to aggregate into nanoparticles with dimensions of 50–1000 nm [28]. Based on this self-assembly property, Gorodetsky et al. fabricated reflectin films that are capable of displaying stimuli-responsive structural colors [57]. They also systemically demonstrated the morphology of the films composed of *Doryteuthis* (*Loligo*) *pealeii* reflectin A1 (RfA1) isoform to reveal the self-assembly process of RfA1 [58]. As shown in Fig. 6a, since RfA1 comprises hydrophilic linker regions and less hydrophilic conserved motifs, the conserved motifs are relatively more confined. Via protein folding, elongated nanoparticles are formed and dispersed in solution under the interaction of electrostatic and hydrophobic forces. When transferred onto a solid substrate and dried, the nanoparticles become oblate and self-assemble into a film, which shows color through thin-film interference (typical reflection spectrum shown in Fig. 6b). This hierarchically-structured film can change its color upon external stimuli (*e.g.* acid vapor) through thickness alteration. Silk fibroin is extracted from *Bombyx mori* silkworm cocoon, through step-by-step purification with reagents of sodium carbonate and lithium bromide. Due to its transparency and mechanical durability, silk fibroin has been introduced to fabricate free-standing structural color film, usually in the manner of silk inverse opal (SIO) structure. A pioneering work of fabricating SIOs was demonstrated by Omenetto et al. [59]. As shown in Fig. 6c, poly(methyl methacrylate) (PMMA) microspheres are firstly self-assembled into opal structure template. Then aqueous fibroin solution is poured into the template. After drying, the composite film is detached from the substrate and immersed in acetone to dissolve PMMA template. The resulting silk film shows porous inverse opal structure and bright color (typical reflection spectrum shown in Fig. 6e). The SIOs can be also chemically crosslinked, leading to stretchable films [60]. Since the silk matrix can be expanded by water, SIOs are good candidates for humidity sensing, even applicable as implantable biosensors [61].

In addition to the proteins, phages are emerging as promising natural materials for structural color sensors. Phages are bacterial viruses that can self-evolve and self-replicate. Composed of a protein coat encapsulated RNA or DNA genome, phages can be easily modified to respond to various targets by engineering the protein coat [62]. By pulling the substrates from M13 phages (filamentous bacterial viruses) solution, Lee et al. achieved films with fiber bundle nanostructures, from self-assembled deposition of the phages (Fig. 6d) [8]. Due to the quasi-ordered M13 phage arrays, the films exhibit angle-independent colors through scattering of light within the nanostructures (typical reflection spectrum shown in Fig. 6e). The colors can be easily tuned by changing the pulling speed, which influences the diameter and interspacing of the nanostructures. Upon external stimuli, the phages can swell or shrink, resulting in the volume change of the nanostructures and thus the color shift.

4. Structural color-based chemical sensors and biosensors

In this section, progresses on the chemical sensing and biosensing of

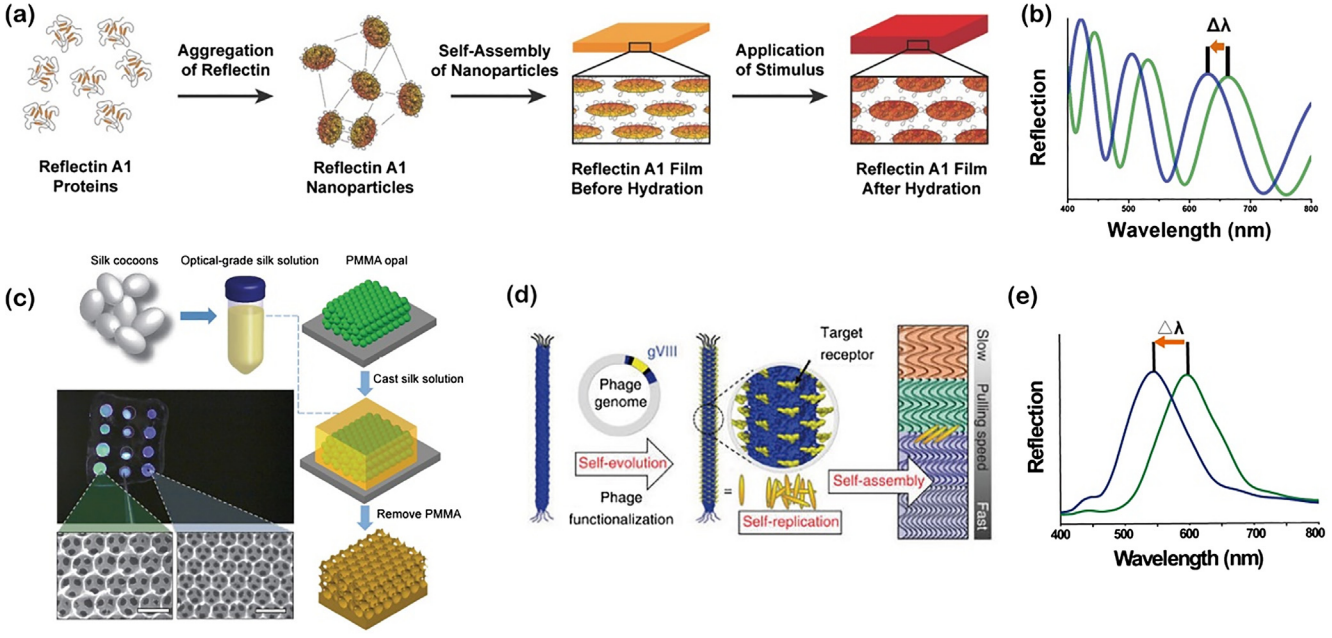

Fig. 6. (a) Self-assembly process of RfA1 and its response to stimuli [58]. (b) Typical reflection spectrum of reflectin self-assembling film. △λ is the shift of the location of constructive interference upon external stimuli. (c) SIO fabricated from PMMA opal structure template [59]. (d) Self-assembly of M13 phages [8]. (e) Typical reflection spectrum of (c) and (d). △λ is the shift of the location of photonic band gap upon external stimuli.

Table 1
Performance of responsive soft materials based structural color sensors.[a]

Analyte		Material and structure	Detection range/Sensitivity	Response time	Selectivity	Ref.
pH		Poly(AAc-*co*-AAm) PC hydrogel	pH 2.2–10.5	/	/	[63]
		Poly(HEA-*co*-AAc) PC hydrogel	210 nm △λ between pH 3.6 and pH 7.2	< 40 ms	/	[64]
Ions	CO_3^{2-}	PAAc hydrogel inverse opal PC	45 nm △λ between 1 mM and 10 mM	/	Against F^-, Cl^-, Br^-, CH_3COO^-, NO_3^-, HCO_3^-, $S_2O_8^{2-}$, HPO_4^{2-}, $C_2O_4^{2-}$	[65]
	Ca^{2+}	CLC polymer	10^{-4}–10^{-2} M	/	Against Na^+, Mg^{2+}, Ca^{2+}, Zn^{2+}, Cd^{2+}	[66]
	Cu^{2+}	Imidazole functionalized hydrogel interferometer	LOD of 10^{-14} M	A few minutes	Against Ag^+, Ba^{2+}, Ca^{2+}, Co^{2+}, Cr^{3+}, Fe^{3+}, Hg^{2+}, K^+, Mg^{2+}, Mn^{2+}, Na^+, Ni^{2+}, Pb^{2+}, Zn^{2+}	[12]
	Be^{2+}	Crown ether functionalized PC hydrogel	LOD of 10^{-11} M in seawater	/	Against Li^+, Na^+, K^+, Fe^{2+}, Ca^{2+}, Co^{2+}, Zn^{2+}, Mg^{2+}	[67]
	Hg^{2+}	Aptamer crosslinked PC hydrogel microcapsule	1–10 μM	/	Highly specific detection	[68]
		-SH groups functionalize PC hydrogel	LOD of 10^{-9} M in seawater	within 20 min	Against Mg^{2+}, Ca^{2+}, Co^{2+}, Cu^{2+}, Zn^{2+}, Ba^{2+}, Pb^{2+}, Cd^{2+}	[69]
Humidity		Poly(AAm-*co*-AAc) hydrogel interferometer	100 nm △λ between RH 80% and 85%	Subsecond scale	/	[9]
		Layer-by-layer deposited polyelectrolyte coatings	△λ > 200 nm for RH 100%	35 ms	/	[70]
		PAAm PC hydrogel	92 nm △λ for RH 95%	2–3 min	/	[71]
		Silk–titanate multilayer	RH 10–80%	About 50 s	/	[72]
Organic compounds	Formaldehyde	PAAm PC hydrogel	7 nm △λ for 0.0030 mol/L in aqueous solution	2 h	Against acetone, dimethyl sulfoxide, *N,N*-dimethylformamide, glucose, sodium acetate, urea, polyethylene glycol, lysine, pyridine	[73]
	Volatile alcohols	Poly(HEMA-*co*-MA) PC hydrogel	△λ > 70 nm for volatile alcohols	> 20 min	Against water, acetone, diethyl ether, chloroform, dichloromethane, benzene, toluene, *p*-xylene	[74]
	Ethanol	PS-*b*-P2VP BCP microsphere	220 nm △λ between 40% and 92% in aqueous solution	10 s	/	[75]
	Chloroform vapor	PS-*b*-PMMA BCP assemblies	250 nm △λ	/	Against poor solvents for PS and PMMA	[76]
	Organic solvents	Poly(MMA-AA-EGDMA)/TiO_2 multilayer	/	2 s	Respond to carbon tetrachloride, ethanol, ethyl acetate, methylene chloride, chloroform	[77]
		Poly(*p*-phenyleneoxide)-cellulose acetate multilayer	/	A few hours	Respond to carbon tetrachloride, benzene, 1,2-dichlorobenzene	[78]
Small biomolecules	Glucose	3-Acrylamidophenylboronic acid functionalized PC hydrogel	75 nm △λ between 3 mM and 20 mM	/	/	[79]
		PBA functionalized PC hydrogel	Naked-eye detection of 0.1 mM	/	Against fructose and galactose	[80]
		PVA contained PBA functionalized PC hydrogel	Linear detection of 0–50 mM	Minute scale	/	[81]
		Glucose/galactose binding protein functionalized PC hydrogel	0.2 μM–10 mM	20 min	Binds D-glucose and D-galactose over D-fructose	[82]
	Mannan (utilized for the detection of *C. albicans*)	Lectin-immobilized PC hydrogel	LOD of 32 CFU/mL	About 100 min	Against *E. coli*	[83]
	Urea	Urease-immobilized interpenetrated CLC-hydrogel network	Color changes at 1.9×10^{-3} M	/	Against glucose, cholesterol, biotin, ascorbic acid	[84]
	GAS	TPL functionalized microgel etalon	LOD of 10^{-5} M	25 min	/	[85]
	Triacylglycerol	Lipase functionalized microgel etalon	1–7 mg/mL	40 min	/	[86]
Proteins and enzyme activities	Con A	Mannose functionalized PC hydrogel	LOD of 0.02 mg/mL	About 8 h	/	[87]
	Lectin proteins	Carbohydrate functionalized PC hydrogels	LOD of 7.5×10^{-8} M for ricin, 2.3×10^{-7} M for jacalin, 3.8×10^{-8} M for Con A	/	/	[88]
	HRP	PBA functionalized hydrogel interferometer	LOD of 10^{-11} mg/mL		Against Cyt C, RNase A, Myo, β-lac A, β-cas, Hemo, BSA	[12]
	β-lactam antibiotic and β-lactamase inhibitor	β-lactamase functionalized PC hydrogel	LOD of 1 μM for β-lactam antibiotic, 0.1 μM for β-lactamase inhibitor	/	Against non-β-lactam antibiotics	[89]
	Phosphorylation by PKA	Peptide substrate modified PC hydrogel	LOD of 0.1 U/μL PKA	2 h	/	[90]

[a] △λ is the shift of reflection peak or valley; LOD is limit of detection; RH is relative humidity.

various structural color sensors since 2014 are summarized, specifically on sensing of pH and ions, humidity and organic compounds, small biomolecules, as well as proteins and enzyme activities (sensing performance summarized in Table 1). We focus on (but not limited to) the sensors based on the synthetic polymers and natural materials discussed above in this section, and further extended to multi-analysis of these targets in the following section.

4.1. pH and ions

Hydrogel-based structural color systems are widely used to detect pH and ionic strength, because these ionic analytes can influence the Donnan osmatic pressure within the networks with charged moieties. Typical electrolyte polymers, such as poly(acrylic acid) (PAAc) hydrogels [63], are often used for sensing of the ionic analytes. Recently, Guan et al. reported Fe_3O_4@polyvinylpyrrolidone@ poly(2-hydroxyethyl acrylate-*co*-acrylic acid) (Fe_3O_4@PVP@poly(HEA-*co*-AAc)) photonic nanochains for pH sensing, based on hydrogen bond-guided template polymerization method [64]. These nanochains are characterized by 1D PC structure immobilized in hydrogel matrix. They are obtained by photo-polymerization of the mixtures of Fe_3O_4@PVP nanoparticles, monomers (HEA and AAc), the cross-linker, and the photo-initiator, under magnetic field. Since the PVP shell of nanoparticles can form hydrogen bonds with hydroxyl and carboxyl groups of HEA and AAc, the monomers concentrate around the nanoparticles. As a result, only these monomers of high concentration can be polymerized, while the rest remains in liquid. As shown in Fig. 7a, the nanochains show structural colors dependent on pH values of the microenvironment. Higher pH induces deprotonation of carboxyl groups of poly(HEA-*co*-AAc) into carboxylates, resulting in the increase of negative charges within the hydrogel matrix and the swelling of the networks. Hence, the lattice spacing of the nanochain increases, giving rise to color change. Attributed to the submicrometer size, the response time is 40 ms, which is 2–3 orders of magnitude smaller than the previous bulk counterpart sensors. This pH-responsiveness of hydrogels can be utilized to detect anions. For example, CO_3^{2-} can be detected by inverse opal-structured PAAc hydrogel networks crosslinked by ethyleneglycol dimethacrylate (EGDMA), since the networks respond to a certain range of pHs, which corresponds to CO_3^{2-} aqueous solutions of concentrations from 1 to 10 mM [65]. Limited to the pH responsiveness, this anion sensor is not highly selective.

Sensing of metal ions by structural color sensors is realized through functionalizing the networks with recognition units. Gu et al. reported highly selective detection of Hg^{2+} by embedding the corresponding aptamer into polyacrylamide (PAAm) immobilized microcapsules [68]. The microcapsule is composed of a core of self-assembled SiO_2 nanoparticles and a shell of aptamer functionalized PAAm hydrogel networks. Specific binding of Hg^{2+} with aptamer causes the shrinking of the networks, resulting in naked-eye sensing signals. CLC polymers has also been used to detect metal ions, reported by Schenning et al. [66]. As shown in Fig. 7b, the CLC polymer is formed by crosslinking mesogens (RM 257 and RM 105) and metal-ion-binding moieties (6OBA and 6OBAM), with photo-initiator Irgacure 369 and chiral dopant MAA. After polymerization, MAA is removed by solvent, to achieve more flexible networks. Then the CLC polymer is treated with KOH solution, which converts the benzoic acid units to potassium benzoate derivatives, to realize the capability of binding metal ions. Among the tested metal ions such as Na^+, Mg^{2+}, Ca^{2+} and Zn^{2+}, Ca^{2+} can induce the most significant decrease of helical pitch length and the blue-shift of reflection. This CLC polymer shows selective and sensitive colorimetric detection of Ca^{2+} with concentrations from 10^{-4} to10^{-2} M in aqueous solution, which covers the range of total blood calcium of a healthy person (2.1×10^{-3} to 2.6×10^{-3} M). Furthermore, Ca^{2+} in serum can be also detected. Hypo blood samples (hypoCa-1 and hypoCa-2, concentrations of Ca^{2+} are reduced), normal serum, and hypercalcemic blood sample (hyperCa, concentration of Ca^{2+} is increased) give rise to different colorimetric signals. Such recognition of metal ions in complex microenvironment is of importance for practical applications and has been achieved with different structural color sensors [67,69]. Ultrahigh sensitivity with microscale sensors is desirable but still challenging for detecting the trace amount of metal ions in real-time health and environment monitoring and disease prescreening. Recently, He et al. have achieved unprecedented femtomol-level sensitivity and high selectivity in copper ion detection with a hydrogel interferometer of micrometer size [12]. This ultrahigh sensitivity is mainly attributed to the in-situ analyte preconcentrating effect due to the local shrinking upon metal ion binding with multiple polymer chains of the hydrogel network (concentrating an analyte droplet as high as 10^9 folds), as well as the significant chemo-mechano-optical signal amplification of the interference. As shown in Fig. 7c, with the increase concentration of Cu^{2+}, the hydrogel interferometer shows shrinkage and blue-shift of the reflection peak; Cu^{2+} with concentration of 10^{-14} M can produce detectable sensing signals. In addition to the ultrahigh sensitivity, the sensor shows high selectivity towards Cu^{2+}, against 14 interfering metal ions, including Ag^+, Ba^{2+}, Ca^{2+}, Co^{2+}, Cr^{3+}, Fe^{3+}, Hg^{2+}, K^+, Mg^{2+}, Mn^{2+}, Na^+, Ni^{2+}, Pb^{2+} and Zn^{2+}, providing great potential for real-life applications with various water or biofluid sources.

4.2. Humidity and organic compounds

Polymeric networks can be significantly swollen by their good solvents, which is the commonly utilized basis of structural color sensors for humidity and organic vapors or solvents. He et al. demonstrated a patterned poly(AAm-*co*-AAc) hydrogel interferometer as a humidity indicator, by spatially controlled polymerization (Figs. 3a and 8a) [9]. Due to the thicknesses difference on the different regions of the patterned hydrogel, the image area and the surrounding area present different interference colors. With increased humidity, these areas undergo thickness increase and color change differently, attributed to diffusion of water molecules into poly(AAm-*co*-AAc) networks. At relatively high humidity, the increased chemical potential of surrounding water vapor boosts the swelling ratio of the hydrogel layer, resulting in sensitive super-linear responsiveness for a small alteration of humidity. By applying poly(2-hydroxyethyl methacrylate-*co*-acrylic acid) (poly (HEMA-*co*-AAc)) as the hydrogel layer, this interferometer shows colorimetric sensing information to organic solvent vapors. Due to submicron thickness of hydrogel layer and strong polymer-solvent affinity, the hydrogel interferometer shows response and recovery time at subsecond scale. Compared with the previously reported hydrogel-based volatile-vapor sensors which show response time of several minutes, this hydrogel interferometer is much faster. Such thin-film interference color based humidity sensor with fast response is also achieved by layer-by-layer deposition of polyelectrolytes, which shows response time of *ca.* 35 ms [70]. In other reported studies, hydrogels are incorporated into PC templates and functionalized to detect humidity [71], and organic vapors or solvents [73,74].

The solvatochromism of BCPs makes them ideal sensors for solvents. BCP microspheres with concentric lamellar structure has been developed by Zhu et al. to sense ethanol [75]. The microspheres are formed by adding chloroform droplets of PS-*b*-P2VP into poly(vinyl alcohol) (PVA) through microfluidics. Due to the affinity of PVA to the pyridine group of P2VP, the P2VP blocks are attracted to the oil/water interface and form the outermost layer of the lamellar structure of BCP assemblies after the evaporation of chloroform solvent (Fig. 8b). With the addition of ethanol, the P2VP microdomains swell remarkably, leading to visible colors in the central part of the microspheres. Increasing concentration of ethanol in aqueous solution from 40% to 92% results in increased swelling of the P2VP microdomains and the color change from blue to red. After removing ethanol, P2VP brushes collapse onto PS layer, leaving concentric cavities and fading of colors, since the hollow structure cannot satisfy the requirements of visible structural colors. This coloration-fading cycle can be repeated. Besides BCP

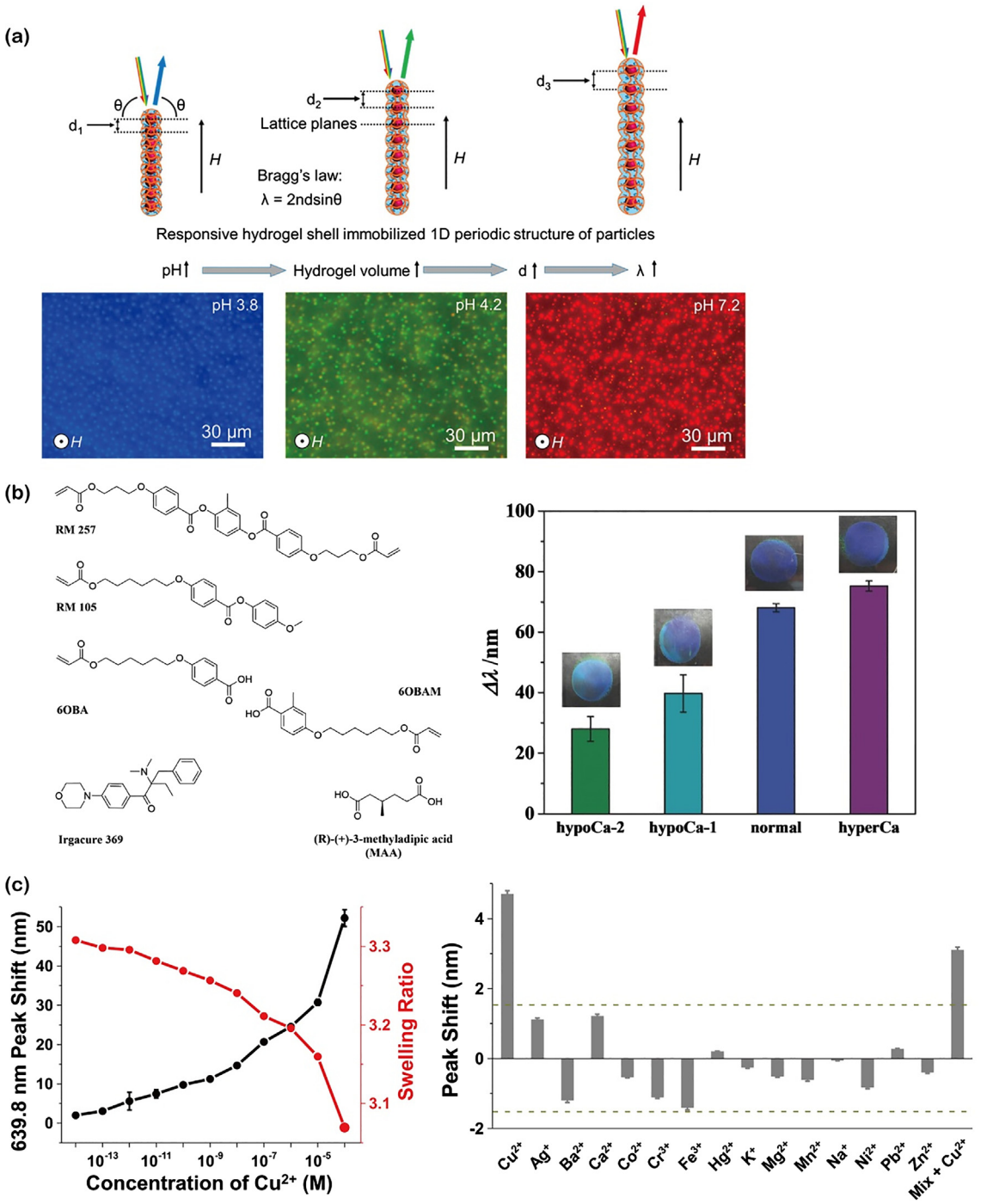

Fig. 7. (a) Fe_3O_4@PVP@poly(HEA-*co*-AAc) photonic nanochains for pH sensing [64]. (b) CLC polymer sensor for detection of Ca^{2+} in serum [66]. (c) Hydrogel interferometer for ultrasensitive and selective detection of Cu^{2+} [12].

assemblies in highly ordered structure, short-range-order PS-*b*-PMMA gyroid structure is developed to serve as an angle-independent sensor for organic compounds [76]. Other lamellar PC structures based on responsive soft materials, for example, composite films with alternatively arranged materials, have also been reported recently for sensing of humidity and organic compounds [72,77,78].

4.3. Small biomolecules

The detection of glucose by structural color sensors has been realized through functionalization of involved polymer networks with binding units, of which the most used is phenylboronic acid (PBA) and its derivatives. PBA can bind with glucose to form boronate ester complex, inducing the diffusion of glucose into polymer; the increased osmotic pressure causes the swelling of polymer networks [79]. However, at low concentration of glucose, one PBA unit can bind with two glucose molecules, forming 2:1 PBA-glucose complex. In this case, the glucose molecules can be considered as cross-linkers, causing the shrinking of polymer networks [80]. To realize structural color sensors for linear response to glucose, Braun et al. developed PBA-incorporated PC hydrogel with “volume resetting agents” PVA to eliminate the formation of 2:1 PBA-glucose complex [81]. As shown in Fig. 9a, the opal-structured PAAm hydrogel is firstly hydrolyzed and treated with PBA, followed by introducing of PVA into the networks. Due to the binding of

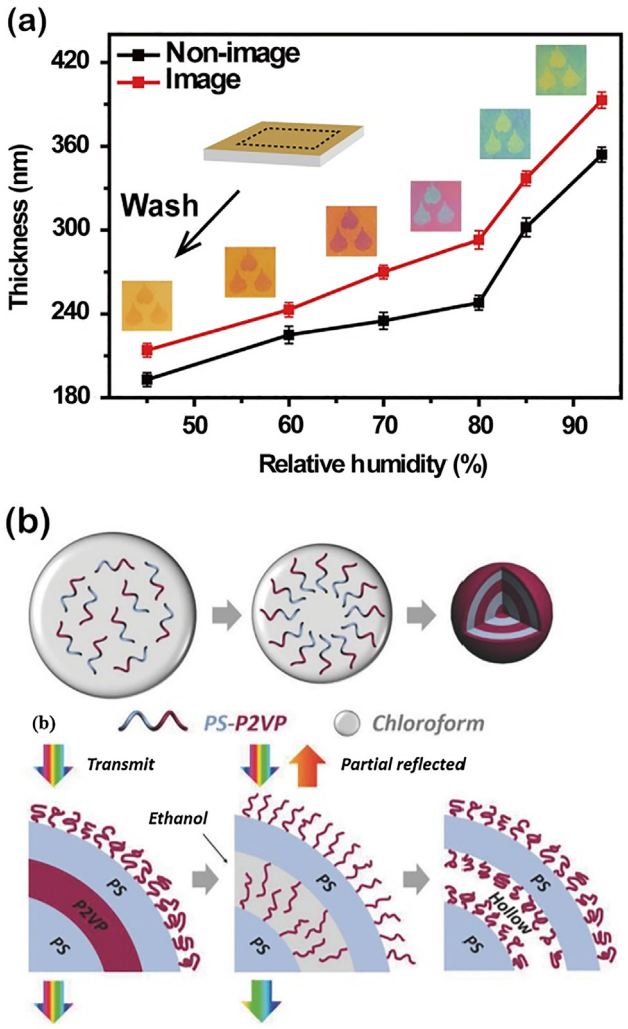

Fig. 8. (a) Patterned hydrogel interferometer for humidity sensing [9]. (b) Sensing of ethanol by BCP microspheres with concentric lamellar structure [75].

PBA with 1,3-diol PVA and hydrogen bonds, the hydrogel shrinks. Since the affinity between PBA and1,2-diol is stronger than that between PBA and 1,3-diol, addition of 1,2-diol glucose leads to displacement of PBA-PVA complex by PBA-glucose complex, resulting in swelling of the networks and red-shift of reflection. Via this strategy, glucose with concentration ranging from 0 to 50 mM can be detected linearly, with response kinetics at minute scale.

In addition to PBA binding units, glucose binding proteins have also been incorporated into PC hydrogels to selectively detect glucose [82]. In fact, due to the strong affinity between specific proteins and saccharides through interactions such as the binding of hydroxyl groups to amino acid residues and/or metal ions, various proteins-immobilized hydrogels can be designed to respond to different saccharides. Asher et al. demonstrated a lectin-immobilized 2D PC hydrogel sensor (structure shown in Fig. 3e) for selective recognition of mannan, and thus they detected *Candida albicans* (*C. albicans*) since mannan were the major surface carbohydrates in *C. albicans* [83]. The hydrogel matrix is formed by crosslinking lectin Concanavalin A (Con A) monomer with glutaraldehyde. Attributed to the Con A-mannan binding, the hydrogel matrix shrinks in the presence of *C. albicans*, giving rise to a blue-shift of reflection and the color change of the sensor. The LOD is as low as 32 CFU/mL which is much lower than the physiologically typical concentration (400 CFU/mL in saliva). Proteins-immobilized hydrogels can also be introduced into CLC polymers to generate structural color sensors, for example, a CLC polymer sensor for urea detection by employing urease-immobilized PAAc hydrogel [84].

Nerve agents are organophosphonates that affect the action of nervous system. By functionalization of microgel etalon (structure shown in Fig. 3b) with triphenylmethane leucohydroxide (TPL), a molecule that could be ionized to produce nucleophilic hydroxy group, Serpe et al. developed a structural color sensor for a nerve agent mimic, diethylcyanophosphate (GAS) [85]. TPL is introduced to copolymerize with *N*-isopropylacrylamide (NIPAm) and *N,N′*-methylenebisacrylamide (MBAm) to form pNIPAm-based microgels. The stimulus of GAS causes the phosphorylation of the TPL hydroxy group, leading to increased electrostatic repulsion within the microgel array and thus the swelling of microgels (Fig. 9b). The resulting red-shift of the reflection peak of microgel etalon is related to the concentration of GAS, showing sensitive detection at the concentration of μM scale. This microgel etalon is GAS selectively responsive, as other related organophosphates, *e.g.* triethyl phosphate, cannot induce peak shift. In addition to sensor for nerve agents, microgel etalon for lipid triacylglycerol is also demonstrated through embedding lipase into the microgels [86].

4.4. Proteins and enzyme activities

The recognition of proteins can be realized by incorporating saccharide moieties into PC hydrogel matrix, due to the strong protein-

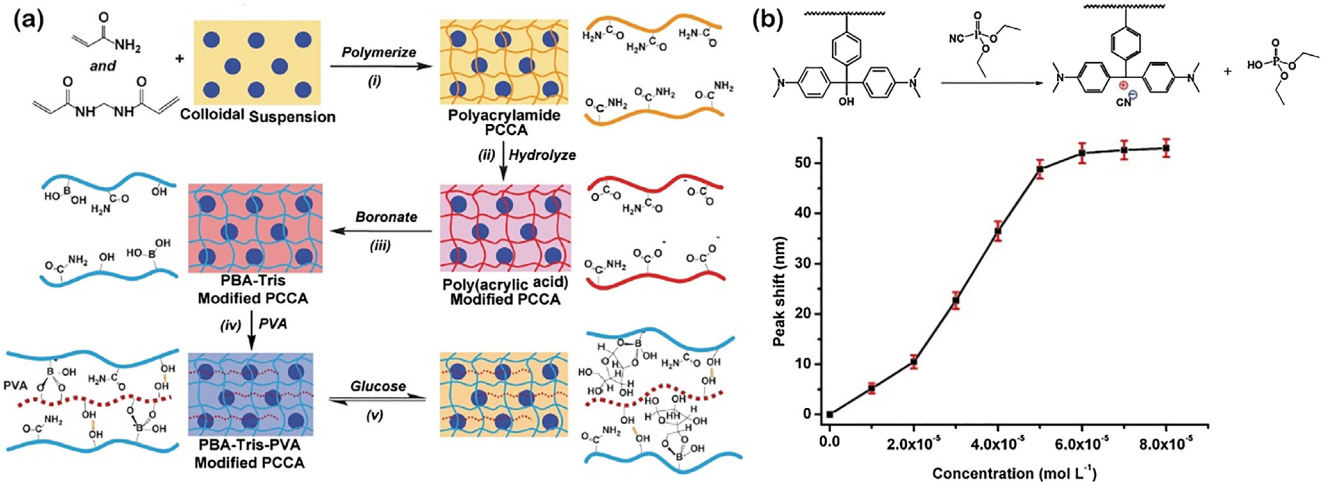

Fig. 9. (a) Linear sensing of glucose by PBA incorporated PC hydrogel with "volume resetting agents" PVA [81]. (b) TPL functionalized microgel etalon for detecting a nerve agent mimic, diethylcyanophosphate (GAS) [85].

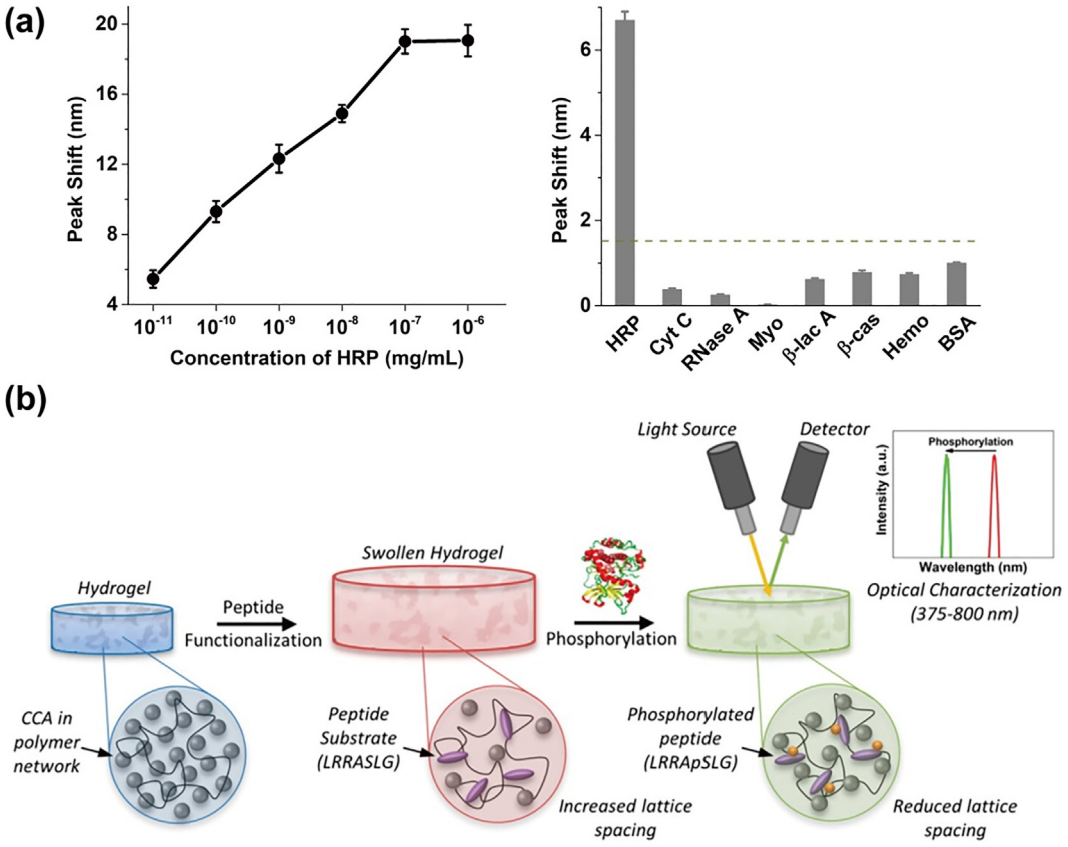

Fig. 10. (a) Sensitive and selective detection of HRP with PBA functionalized hydrogel interferometer [12]. (b) Peptide substrate modified PC hydrogel sensor to monitor PKA activity [90].

saccharide affinity mentioned above. Asher et al. reported various saccharides modified 2D PC hydrogels (structure shown in Fig. 3e) to detect different proteins [87,88]. To create responsive hydrogels, saccharide groups contained monomers are added to the copolymerization. With stimuli of proteins, protein-saccharide binding causes shrinkage of hydrogels and blue-shift of reflection. The 2D PC hydrogel sensors are selective, exhibiting responsiveness as lactose modified sensor to ricin, α-galactose modified sensor to jacalin, and mannose modified sensor to Con A. This saccharide-modified hydrogel sensor provides a facile and cost-effective approach to the detection of proteins. By functionalizing polymer chains with PBA ligands, He et al. used the hydrogel interferometer to detect glycoproteins peroxidase from horseradish (HRP) [12]. The PBA ligands can bind diols in the glycoprotein, forming a 1:1 complex. The increase of anionic boronate species in the hydrogel upon binding with glycoproteins leads to hydrogel swelling and red-shift of the reflection wavelength. As shown in Fig. 10a, this sensor can realize sensitive detection of HRP, showing LOD of *ca.* 10^{-11} mg/mL and great selectivity over seven interfering proteins. Enzyme-immobilized PC hydrogel sensors are the alternative for highly-selective recognition of proteins and corresponding enzyme inhibitors. An example has been demonstrated by incorporating β-lactamase into 3D PC hydrogel to result in naked-eye sensing of β-lactam antibiotic and β-lactamase inhibitor [89].

Contrary to introducing enzyme into hydrogel sensor for substrate proteins, incorporating substrate into hydrogel matrix can be used for the monitoring of enzyme activity. Kaar et al. reported a peptide substrate (LRRASLG) modified PC hydrogel sensor to monitor phosphorylation by protein kinase A (PKA) [90]. As shown in Fig. 10b, the positively charged peptide substrate is incorporated to the hydrogel matrix by using click chemistry, leading to the swelling of the hydrogel. The addition of PKA causes phosphorylation of the peptide substrate, generating negative charges within hydrogel matrix and thus shrinkage of the networks. Hence, the kinase activity can be detected by observing blue-shift of reflection of the PC hydrogel sensor. The sensitivity to PKA is related to the concentration of immobilized peptide, as addition of 1 mM peptide can realize sensitivity of 0.5 U/μL, while 10 mM peptide can achieve sensitivity of 0.1 U/μL.

5. Structural color sensor array for multi-analyte discrimination

Discrimination of multi-analyte by sensor arrays has attracted much attention in recent years. To achieve facile discrimination, the design of sensor arrays is focused on involving less sensing materials to obtain sufficient sensing information for all analytes [91–93]. Taking advantage of non-specific interactions between sensing motif and targeting analytes to generate cross-reactive responses, single-material based structural color sensor arrays have been developed. A simple and universal strategy has been demonstrated by He et al. [9]. Via integration of poly(HEMA-*co*-AAc) based hydrogel interferometers with different hydrogel thicknesses into a sensor array, various volatile organic compounds (VOCs) can be distinguished (Fig. 11a). On the basis of different swelling behaviors of the hydrogel in different vapors, the single-hydrogel based sensor array shows varied color patterns to the eight different vapors including acetone, ethanol, acetic acid, hexane, *etc*. Through collection and analysis of the RGB color patterns, eight VOCs are discriminated. To facilitate commercial application, smartphone based colorimetric analysis system has been established, which directly shows the result of VOCs identification.

Attributed to vapor response of genetically engineered M13 phage [8], Oh et al. reported a M13 phage based sensor array for the recognition of multiple cells [94]. Through genetic modification, M13 phage expresses a tryptophan (W)–histidine (H)–tryptophan (W)–glutamine (Q) sequence of amino acids in the major coat protein (Fig. 11b). By self-assembly of the phages, a sensor array with red,

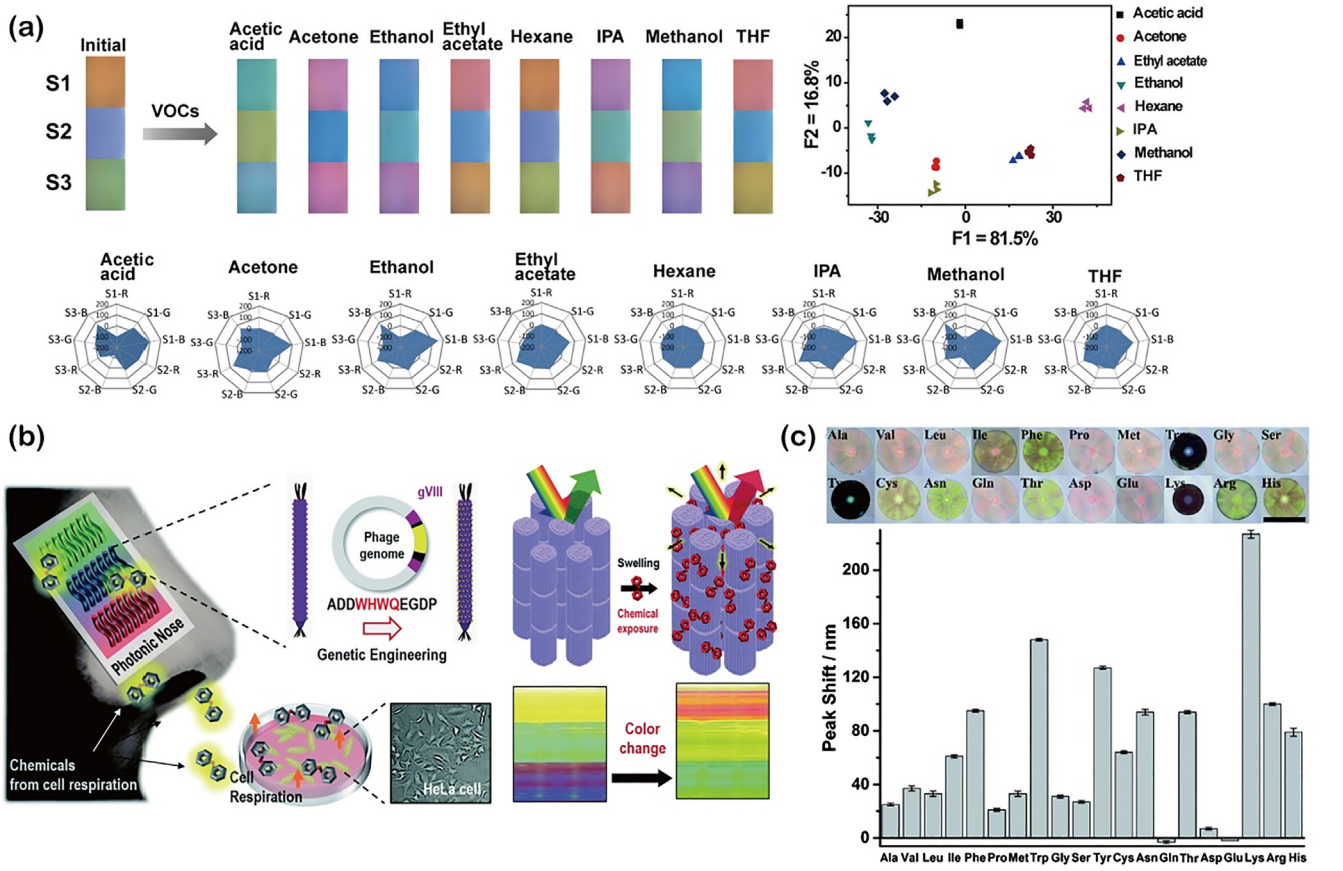

Fig. 11. Sensor arrays for multi-analyte discrimination. (a) VOCs discrimination by poly(HEMA-*co*-AAc) based sensor array of hydrogel interferometers with different hydrogel thicknesses [9]. (b) Genetically engineered M13 phage sensor array for discrimination of multiple cells [94]. (c) PIL inverse opal sphere arrays for recognition of twenty natural amino acids [96].

green, and blue bands are achieved. Due to π-π interactions between the WHWQ sequence and VOCs exhaled by cells, the M13 phage assembled array would be swollen or shrunken by the VOCs, giving rise to differential color patterns to diverse cells. This single-phage based sensor array is capable of discriminate five cell lines.

Utilizing the sensitivity of imidazolium-based poly(ionic liquid) (PIL) to external environment [95], Li et al. demonstrated PIL-incorporated inverse opal photonic spheres for the recognition of amino acids [96]. The photonic spheres are obtained by the polymerization of IL monomers in the voids of PC template from SiO_2 nanoparticles self-assembly, which are formed through microfluidics, and then etching of the template. Due to multiple molecular interactions within the imidazolium-based ILs, including van der Waals forces, electrostatic forces, hydrogen bonding, hydrophobic interactions, and π-π interactions, the PIL inverse opal spheres show different interactions with various amino acids. As shown in Fig. 11c, the photonic spheres exhibit different swelling behaviors in solutions of twenty natural amino acids, leading to distinguishable structural colors and reflection peak shift to the amino acids. Despite that aggregation-induced emission dye is introduced into the spheres for fluorescence-based detection, the identification of amino acids (concentration of 10 mM) can be realized with their characteristic colorimetric signals generating by this single-PIL inverse opal sphere array.

6. Summary and outlook

In this review article, we have summarized the design of promising responsive soft materials-based structural color sensors, as well as their recent applications for chemicals sensing, biosensing, and array-based sensing for multi-analyte. Learning from living organisms, diverse photonic structures can be mimicked, among which responsive soft material-involved photonic structures show large volumetric change, leading to remarkable and sensitive color alteration. Synthetic polymers and some natural materials are the most studied and utilized soft materials for structural color sensors, attributed to their stimuli-responsive volume change and easy functionalization. Through diverse strategies of introducing these materials into photonic structures, colorimetric signals responsive to external stimuli can be achieved. Sensitivity and selectivity can be improved by employing specific binding units into the materials, such as crosslinking with highly-specific monomers and embedding enzymes or aptamers within the materials. On the other hand, cross-reactive structural sensor arrays can be realized with a single material, providing a powerful sensing capability to multi-analyte.

To promote practical and commercial applications of responsive soft material-based structural color sensors, several aspects are desirable to be considered. First, advancing sensing materials to boost the sensing performance to ultrafast response, high durability and sensitivity, to meet the requirement of real-time monitoring of a large variety of analytes. As most practical detections without pre-treatment are performed in complex environment, it is also important to assess the sensing performance against interference such as temperature, humidity, light, and other molecules. Second, integrating sensors with different or cross-reactive responsiveness into a miniaturized sensor chip, and importing the sensing information into smart devices to provide comprehensive analysis of health and environment conditions. In this case, high-resolution patterning of the sensors on the substrate is significant, which includes a number of fundamental issues, for example, control of substrate wettability to enable localization of sensing materials. Third, developing programmable fabrication of these structural color sensors

to realize high reproducibility and large-scale production. Currently, manufacturing technologies such as inkjet printing, 3D printing and microfluidics, have already been applied for the fabrication of structural color sensors. Fourth, exploring new mechanism of producing and detecting structure-induced coloration. For coloration production, responsive soft materials incorporated sensing systems based on tunable interference and diffraction of light has demonstrated their great potential in sensitive colorimetric sensing. Recently, responsive soft materials systems that lead to scattering of light by surface roughness change in the presence of stimuli, more specifically, by forming wrinkle/crease at the surface of materials, are emerging as a new class of structural colorimetric sensors [16,97–103]. For the color detection methods, besides the optical spectrometry and the RGB color analysis for quantitative analyte detection, naked eye sensing mode is also becoming useful with the booming of the artificial intelligence and smart phone-based technologies. Phone App based chemical sensing has been demonstrated [7–9], showing potentials for remote data collection, which benefits bioinformatics and real-time monitoring in public health, environment, and security fields. Advancement of these and new technologies can remarkably facilitate the commercialization of the sensors. The future structural color sensors are promising in daily health monitoring and noninvasive diagnostic screening, by detecting exhaled breath, tears, sweat, or saliva. The sensors that are wearable or integratable into fabrics for visual detection of environmental gases can be applied in industry and military affairs, for example, wearable sensors for coal miners to monitor concentrations of oxygen and explosive gases. On the basis that sensing signals of responsive soft material-based structural colors sensors are visual, readable and sensitive, the sensors can significantly contribute to a wide range of future applications. Extending the color response of structural color sensors to invisible spectral region, *e.g.* infrared region, will benefit the design of devices for camouflage, anti-counterfeiting, display, data encryption and information storage, modification, and readout.

Acknowledgements

This work was supported by NSF award 1724526, AFOSR Grant FA9550-17-1-0311, ONR award N000141712117, and UCLA Faculty Research Grant.

References

[1] W. Gao, S. Emaminejad, H.Y.Y. Nyein, S. Challa, K. Chen, A. Peck, H.M. Fahad, H. Ota, H. Shiraki, D. Kiriya, D.-H. Lien, G.A. Brooks, R.W. Davis, A. Javey, Nature 529 (2016) 509–514.
[2] H. Yu, W.W. Jing, R. Iriya, Y.Z. Yang, K. Syal, M.N. Mo, T.E. Grys, S.E. Haydel, S.P. Wang, N.J. Tao, Anal. Chem. 90 (2018) 6314–6322.
[3] C.W. Lin, Y. Zhu, J.J. Yu, X.C. Qin, X.J. Xian, F. Tsow, E.S. Forzani, D. Wang, N.J. Tao, Anal. Chem. 90 (2018) 5375–5380.
[4] T.M. Swager, Angew. Chem. Int. Ed. 57 (2018) 4248–4257.
[5] R.A. Potyrailo, Chem. Rev. 116 (2016) (1923) 11877–11881.
[6] I. Golnaz, L. Marco, Adv. Mater. 30 (2018) 1707069.
[7] J.H. Lee, B. Fan, T.D. Samdin, D.A. Monteiro, M.S. Desai, O. Scheideler, H.-E. Jin, S. Kim, S.-W. Lee, ACS Nano 11 (2017) 3632–3641.
[8] J.-W. Oh, W.-J. Chung, K. Heo, H.-E. Jin, B.Y. Lee, E. Wang, C. Zueger, W. Wong, J. Meyer, C. Kim, S.-Y. Lee, W.-G. Kim, M. Zemla, M. Auer, A. Hexemer, S.-W. Lee, Nat. Commun. 5 (2014) 3043.
[9] M. Qin, M. Sun, R. Bai, Y. Mao, X. Qian, D. Sikka, Y. Zhao, H.J. Qi, Z. Suo, X. He, Adv. Mater. 30 (2018) 1800468.
[10] S.M. Borisov, O.S. Wolfbeis, Chem. Rev. 108 (2008) 423–461.
[11] X. Zhou, S. Lee, Z. Xu, J. Yoon, Chem. Rev. 115 (2015) 7944–8000.
[12] M. Sun, R. Bai, X. Yang, J. Song, M. Qin, Z. Suo, X. He, Adv. Mater. (2018) 1804916.
[13] B. Kaur, N. Kaur, S. Kumar, Coordin. Chem. Rev. 358 (2018) 13–69.
[14] L. Tang, J. Li, ACS Sensors 2 (2017) 857–875.
[15] C. Fenzl, T. Hirsch, O.S. Wolfbeis, Angew. Chem. Int. Ed. 53 (2014) 3318–3335.
[16] C. Xu, G.T. Stiubianu, A.A. Gorodetsky, Science 359 (2018) 1495–1500.
[17] E. Shevtsova, C. Hansson, D.H. Janzen, J. Kjaerandsen, Proc. Natl. Acad. Sci. USA 108 (2011) 668–673.
[18] L.P. Wu, J.Q. He, W. Shang, T. Deng, J.J. Gu, H.L. Su, Q.L. Liu, W. Zhang, D. Zhang, Adv. Opt. Mater. 4 (2016) 195–224.
[19] F. Liu, B.Q. Dong, X.H. Liu, Y.M. Zheng, J. Zi, Opt. Express 17 (2009) 16183–16191.
[20] H.M. Whitney, M. Kolle, P. Andrew, L. Chittka, U. Steiner, B.J. Glover, Science 323 (2009) 130–133.
[21] V. Welch, J.P. Vigneron, V. Lousse, A. Parker, Phys. Rev. E 73 (2006) 041916.
[22] A.R. Parker, V.L. Welch, D. Driver, N. Martini, Nature 426 (2003) 786–787.
[23] J.W. Galusha, L.R. Richey, J.S. Gardner, J.N. Cha, M.H. Bartl, Phys. Rev. E 77 (2008) 050904(R).
[24] R.W. Corkery, E.C. Tyrode, Interface Focus 7 (2017) 20160154.
[25] L. Han, S.A. Che, Adv. Mater. 30 (2018) 1705708.
[26] J.H. Kim, J.H. Moon, S.-Y. Lee, J. Park, Appl. Phys. Lett. 97 (2010) 103701.
[27] J. Teyssier, S.V. Saenko, D. van der Marel, M.C. Milinkovitch, Nat. Commun. 6 (2015) 6368.
[28] R.M. Kramer, W.J. Crookes-Goodson, R.R. Naik, Nat. Mater. 6 (2007) 533.
[29] H.-B. Seo, S.-Y. Lee, Sci. Rep. 7 (2017) 44927.
[30] R. Hanlon, Curr. Biol. 17 (2007) R400–R404.
[31] J.P. Ge, Y.D. Yin, Angew. Chem. Int. Ed. 50 (2011) 1492–1522.
[32] A. Doring, W. Birnbaum, D. Kuckling, Chem. Soc. Rev. 42 (2013) 7391–7420.
[33] D. Buenger, F. Topuz, J. Groll, Prog. Polym. Sci. 37 (2012) 1678–1719.
[34] M.L. Wei, Y.F. Gao, X. Li, M.J. Serpe, Polym. Chem. 8 (2017) 127–143.
[35] L. Hu, M.J. Serpe, ACS Appl. Mater. Interfaces 5 (2013) 11977–11983.
[36] M.S. Wang, Y.D. Yin, J. Am. Chem. Soc. 138 (2016) 6315–6323.
[37] R.M. Parker, G. Guidetti, C.A. Williams, T.H. Zhao, A. Narkevicius, S. Vignolini, B. Frka-Petesic, Adv. Mater. 30 (2018) 1704477.
[38] Y. Kun, M. Qijun, B. Vincent, Z. Qi, Adv. Mater. 29 (2017) 1701323.
[39] A.P.C. Almeida, J.P. Canejo, S.N. Fernandes, C. Echeverria, P.L. Almeida, M.H. Godinho, Adv. Mater. 30 (2018) 1703655.
[40] J.-T. Zhang, L. Wang, J. Luo, A. Tikhonov, N. Kornienko, S.A. Asher, J. Am. Chem. Soc. 133 (2011) 9152–9155.
[41] C.H. Liu, G.Z. Gao, Y.Q. Zhang, L.B. Wang, J.X. Wang, Y.L. Song, Macromol. Rapid Commun. 33 (2012) 380–385.
[42] Y. Zhao, L. Shang, Y. Cheng, Z. Gu, Acc. Chem. Res. 47 (2014) 3632–3642.
[43] L.B. Wang, J.X. Wang, Y. Huang, M.J. Liu, M.X. Kuang, Y.F. Li, L. Jiang, Y.L. Song, J. Mater. Chem. 22 (2012) 21405–21411.
[44] Z. Cai, N.L. Smith, J.-T. Zhang, S.A. Asher, Anal. Chem. 87 (2015) 5013–5025.
[45] D.J. Mulder, A. Schenning, C.W.M. Bastiaansen, J. Mater. Chem. C 2 (2014) 6695–6705.
[46] P.V. Shibaev, J. Madsen, A.Z. Genack, Chem. Mater. 16 (2004) 1397–1399.
[47] P.V. Shibaev, K. Schaumburg, V. Plaksin, Chem. Mater. 14 (2002) 959–961.
[48] Chin-Kai Chang, Cees M.W. Bastiaansen, Dirk J. Broer, Hui-Lung Kuo, Adv. Funct. Mater. 22 (2012) 2855–2859.
[49] J.E. Stumpel, E.R. Gil, A.B. Spoelstra, C.W.M. Bastiaansen, D.J. Broer, A. Schenning, Adv. Funct. Mater. 25 (2015) 3314–3320.
[50] Y. Fink, A.M. Urbas, M.G. Bawendi, J.D. Joannopoulos, E.L. Thomas, J. Lightwave Technol. 17 (1999) 1963–1969.
[51] C. Park, J. Yoon, E.L. Thomas, Polymer 44 (2003) 6725–6760.
[52] J.K.D. Mapas, T. Thomay, A.N. Cartwright, J. Ilavsky, J. Rzayev, Macromolecules 49 (2016) 3733–3738.
[53] B.R. Sveinbjornsson, R.A. Weitekamp, G.M. Miyake, Y. Xia, H.A. Atwater, R.H. Grubbs, Proc. Natl. Acad. Sci. USA 109 (2012) 14332–14336.
[54] G.M. Miyake, V.A. Piunova, R.A. Weitekamp, R.H. Grubbs, Angew. Chem. Int. Ed. 51 (2012) 11246–11248.
[55] C. Kang, E. Kim, H. Baek, K. Hwang, D. Kwak, Y. Kang, E.L. Thomas, J. Am. Chem. Soc. 131 (2009) 7538+.
[56] E.-L. Lin, W.-L. Hsu, Y.-W. Chiang, ACS Nano 12 (2018) 485–493.
[57] L. Phan, W.G. Walkup, D.D. Ordinario, E. Karshalev, J.-M. Jocson, A.M. Burke, A.A. Gorodetsky, Adv. Mater. 25 (2013) 5621–5625.
[58] K.L. Naughton, L. Phan, E.M. Leung, R. Kautz, Q. Lin, Y. Van Dyke, B. Marmiroli, B. Sartori, A. Arvai, S. Li, M.E. Pique, M. Naeim, J.P. Kerr, M.J. Aquino, V.A. Roberts, E.D. Getzoff, C. Zhu, S. Bernstorff, A.A. Gorodetsky, Adv. Mater. 28 (2016) 8405–8412.
[59] S. Kim, A.N. Mitropoulos, J.D. Spitzberg, H. Tao, D.L. Kaplan, F.G. Omenetto, Nat. Photon. 6 (2012) 817–822.
[60] K. Min, S. Kim, S. Kim, Proc. Natl. Acad. Sci. USA 114 (2017) 6185–6190.
[61] Y.Y. Diao, X.Y. Liu, G.W. Toh, L. Shi, J. Zi, Adv. Funct. Mater. 23 (2013) 5373–5380.
[62] R. Peltomaa, I. López-Perolio, E. Benito-Peña, R. Barderas, M.C. Moreno-Bondi, Anal. Bioanal. Chem. 408 (2016) 1805–1828.
[63] X. Fei, T. Lu, J. Ma, W.L. Wang, S.M. Zhu, D. Zhang, ACS Appl. Mater. Interfaces 8 (2016) 27091–27098.
[64] W. Luo, Q. Cui, K. Fang, K. Chen, H. Ma, J. Guan, Nano Lett. (2018).
[65] L. Li, B. Zhao, Y. Long, J.-M. Gao, G. Yang, C.-H. Tung, K. Song, J. Mater. Chem. C 3 (2015) 9524–9527.
[66] M. Moirangthem, R. Arts, M. Merkx, A. Schenning, Adv. Funct. Mater. 26 (2016) 1154–1160.
[67] J.J. Qin, B.H. Dong, L.X. Cao, W. Wang, J. Mater. Chem. C 6 (2018) 4234–4242.
[68] Y. Baofen, D. Haibo, C. Yao, G. Hongcheng, Z. Yuanjin, X. Zhuoying, G. Zhongze, Adv. Mater. 26 (2014) 3270–3274.
[69] J.J. Qin, B.H. Dong, X. Li, J.W. Han, R.J. Gao, G. Su, L.X. Cao, W. Wang, J. Mater. Chem. C 5 (2017) 8482–8488.
[70] L. Yu, H. Xu, T.M. Monro, D.G. Lancaster, Y. Xie, H. Zeng, G.Y. Chen, X. Liu, Mater. Horiz. 4 (2017) 72–82.
[71] T. Lu, H. Pan, J. Ma, Y. Li, S.W. Bokhari, X.L. Jiang, S.M. Zhu, D. Zhang, ACS Appl. Mater. Interfaces 9 (2017) 18231–18237.
[72] E. Colusso, G. Perotto, Y. Wang, M. Sturaro, F. Omenetto, A. Martucci, J. Mater. Chem. C 5 (2017) 3924–3931.
[73] X.L. Jia, T. Zhang, J.Y. Wang, K. Wang, H.Y. Tan, Y.D. Hu, L.B. Zhang, J.T. Zhu, Langmuir 34 (2018) 3987–3992.

[74] J. Liu, Y. Zhang, R. Zhou, L. Gao, J. Mater. Chem. C 5 (2017) 6071–6078.
[75] Y. Yang, H. Kim, J. Xu, M.S. Hwang, D. Tian, K. Wang, L. Zhang, Y. Liao, H.G. Park, G.R. Yi, X. Xie, J. Zhu, Adv. Mater. 30 (2018) 1707344.
[76] C.-S. Wu, P.-Y. Tsai, T.-Y. Wang, E.-L. Lin, Y.-C. Huang, Y.-W. Chiang, Anal. Chem. 90 (2018) 4847–4855.
[77] D. Kou, S. Zhang, J.L. Lutkenhaus, L. Wang, B. Tang, W. Ma, J. Mater. Chem. C 6 (2018) 2704–2711.
[78] P. Lova, C. Bastianini, P. Giusto, M. Patrini, P. Rizzo, G. Guerra, M. Iodice, C. Soci, D. Comoretto, A.C.S. Appl, Mater. Interfaces 8 (2016) 31941–31950.
[79] X.D. Hong, Y. Peng, J.L. Bai, B.A. Ning, Y.Y. Liu, Z.J. Zhou, Z.X. Gao, Small 10 (2014) 1308–1313.
[80] F. Xue, Z. Meng, F. Wang, Q. Wang, M. Xue, Z. Xu, J. Mater. Chem. A 2 (2014) 9559–9565.
[81] C. Zhang, G.G. Cano, P.V. Braun, Adv. Mater. 26 (2014) 5678–5683.
[82] Z. Cai, L.A. Luck, D. Punihaole, J.D. Madura, S.A. Asher, Chem. Sci. 7 (2016) 4557–4562.
[83] Z. Cai, D.H. Kwak, D. Punihaole, Z. Hong, S.S. Velankar, X. Liu, S.A. Asher, Angew. Chem. Int. Ed. 54 (2015) 13036–13040.
[84] K.G. Noh, S.Y. Park, Adv. Funct. Mater. 28 (2018) 1707562.
[85] Q.M. Zhang, W. Xu, M.J. Serpe, Angew. Chem. Int. Ed. 53 (2014) 4827–4831.
[86] Q.M. Zhang, D. Berg, S.M. Mugo, M.J. Serpe, Chem. Commun. 51 (2015) 9726–9728.
[87] J.-T. Zhang, Z. Cai, D.H. Kwak, X. Liu, S.A. Asher, Anal. Chem. 86 (2014) 9036–9041.
[88] Z.Y. Cai, A. Sasmal, X.Y. Liu, S.A. Asher, ACS Sensors 2 (2017) 1474–1481.
[89] F. Xiao, G. Li, Y. Wu, Q. Chen, Z. Wu, R. Yu, Anal. Chem. 88 (2016) 9207–9212.
[90] K.I. MacConaghy, D.M. Chadly, M.P. Stoykovich, J.L. Kaar, Anal. Chem. 87 (2015) 3467–3475.
[91] M. Qin, Y. Huang, F.Y. Li, Y.L. Song, J. Mater. Chem. C 3 (2015) 9265–9275.
[92] M. Qin, Y. Huang, Y.N. Li, M. Su, B.D. Chen, H. Sun, P.Y. Yong, C.Q. Ye, F.Y. Li, Y.L. Song, Angew. Chem. Int. Ed. 55 (2016) 6911–6914.
[93] M. Qin, F.Y. Li, Y. Huang, W. Ran, D. Han, Y.L. Song, Anal. Chem. 87 (2015) 837–842.
[94] J.-S. Moon, W.-G. Kim, D.-M. Shin, S.-Y. Lee, C. Kim, Y. Lee, J. Han, K. Kim, S.Y. Yoo, J.-W. Oh, Chem. Sci. 8 (2017) 921–927.
[95] J. Cui, W. Zhu, N. Gao, J. Li, H. Yang, Y. Jiang, P. Seidel, B.J. Ravoo, G. Li, Angew. Chem. Int. Ed. 53 (2014) 3844–3848.
[96] W. Zhang, N. Gao, J. Cui, C. Wang, S. Wang, G. Zhang, X. Dong, D. Zhang, G. Li, Chem. Sci. 8 (2017) 6281–6289.
[97] W. Hong, X. Zhao, Z. Suo, Appl. Phys. Lett. 95 (2009) 111901.
[98] N. Bowden, S. Brittain, A.G. Evans, J.W. Hutchinson, G.M. Whitesides, Nature 393 (1998) 146.
[99] C. Dinesh, A.J. Crosby, Adv. Mater. 23 (2011) 3441–3445.
[100] M. Guvendiren, J.A. Burdick, S. Yang, Soft Matter 6 (2010) 2044–2049.
[101] G. Murat, Y. Shu, J.A. Burdick, Adv. Funct. Mater. 19 (2009) 3038–3045.
[102] K. Philseok, H. Yuhang, A. Jack, K. Mathias, S. Zhigang, A. Joanna, Adv. Opt. Mater. 1 (2013) 381–388.
[103] Y. Shu, K. Krishnacharya, L. Pei-Chun, Adv. Funct. Mater. 20 (2010) 2550–2564.